Mathematics

Research article

New solitary waveforms and their dynamics in the stochastic generalized Chen–Lee–Liu model

Ahmed M. Elsherbeny[1], Taher A. Nofal[2], Yakup Yıldırım[3,4,*] and Ahmed H. Arnous[5]

[1] Department of Physics and Mathematics Engineering, Faculty of Engineering, Ain Shams University, Cairo 11517, Egypt

[2] Department of Mathematics, College of Science, Taif University, P.O. Box 11099, Taif 21944, Saudi Arabia

[3] Department of Computer Engineering, Biruni University, Istanbul 34010, Turkey

[4] Mathematics Research Center, Near East University, Nicosia 99138, Cyprus

[5] Department of Physics and Engineering Mathematics, Higher Institute of Engineering, El–Shorouk Academy, Cairo, Egypt

* **Correspondence:** Email: yyildirim@biruni.edu.tr.

Abstract: This paper explores the dynamics of the generalized Chen-Lee-Liu equation, a fundamental model in nonlinear optics, extended to incorporate multiplicative white noise. By employing Itô calculus, the stochastic behavior of the system was is rigorously analyzed, providing insights into the effects of perturbations on soliton dynamics. The improved extended modified tanh-function approach was utilized to derive a variety of soliton solutions, including singular, dark, and bright solitons, as well as newly identified straddled solitons. This analytical approach highlights the transformative relationships between soliton types under specific conditions, expanding the spectrum of known solutions. The incorporation of multiplicative white noise reveals intricate changes in soliton stability, amplitude, and velocity, illustrating the interplay between deterministic and stochastic influences. These findings offer theoretical advancements in the understanding of soliton behavior in noisy environments and have practical implications for optical communication systems and nonlinear wave modeling. This study enriches the theoretical landscape of soliton dynamics and sets the stage for future research into stochastic soliton systems.

1. Introduction

The study of optical solitons has gained increasing relevance in modern communication technologies due to their potential applications in optical fiber communications and their significant role in driving technological advancement in this field. A range of mathematical frameworks, including the nonlinear Schrödinger equation (NLSE) [1–3], the complex Ginzburg-Landau equation [4–6], the Gerdjikov–Ivanov equation [7], and the Lakshmanan-Porsezian-Daniel model [8,9], have been employed to explore this fascinating subject. These models have been crucial in advancing our understanding of the intricate dynamics involved, emphasizing the significance of mathematical approaches in studying soliton propagation. This collective effort contributes to the exploration of the critical roles of optical solitons, both in providing essential support for the needs of the modern telecommunications industry and in enhancing the frameworks of social media communications, making these theoretical tools indispensable in the field.

The Chen-Lee-Liu (CLL) equation, a significant nonlinear wave equation, was introduced in applied mathematics and theoretical physics to describe certain wave phenomena. It was first presented in the paper by Chen, Lee, and Liu [10]. This work laid the foundation for further exploration and analysis in the propagation of waves under specific conditions and has been influential in studies related to soliton solutions and integrable systems. The CLL equation exemplifies a significant milestone in nonlinear wave dynamics, with a particular focus on soliton solutions, representing a critical evolution or refinement of the NLSE to more accurately reflect certain physical conditions, notably in the fields of optics and hydrodynamics. Understanding the CLL equation necessitates a preliminary appreciation of the NLSE's capacity to model wave packets in nonlinear media, where dispersion and nonlinearity collectively foster soliton formation, stable, localized wave packets that retain their shape while traveling at a constant velocity, applicable across a broad spectrum from fiber optics to quantum condensates, and tsunami analysis. While the original CLL article is a key resource for foundational understanding and applications, subsequent studies have expanded this work, providing analytical solutions, numerical simulations, and experimental validations highlighting the equation's significance in elucidating complex wave phenomena in nonlinear mediums [11–14]. It's imperative to note that the specifics of the citation for the original CLL work are not provided here, but for those interested, academic databases and journals focusing on nonlinear science, applied mathematics, and optical physics are recommended resources. This consolidation underscores the CLL equation's pivotal role in enhancing our understanding of nonlinear wave dynamics, emphasizing the ongoing impact of Chen, Lee, and Liu's contributions to physics and applied mathematics.

In recent years, researchers have been growing interest in studying the effects of adding multiplicative white noise to various nonlinear evolution equations [15–19]. Examining the influence of multiplicative white noise on solitons presents an intriguing area of exploration within the broader realm of nonlinear science and soliton theory. Multiplicative white noise, a stochastic process in which the noise intensity can vary with the system's state, adds a layer of complexity to the dynamics and stability of solitons. Recent works [20,21] have investigated the modulation instability and dynamical behavior of nonlinear evolution equations under the influence of noise, offering insights into the resilience of solitons in stochastic environments. Solitons are self-reinforcing solitary wave packets that maintain their shape while traveling at a constant velocity and are inherently resilient

against perturbations. However, when exposed to multiplicative white noise, these waveforms experience random fluctuations in their propagation characteristics. This can result in amplitude, velocity, and shape variations, potentially affecting their stability and coherence. Understanding these effects is vital, as it can shed light on the resilience of solitons under realistic conditions where noise is an inevitable factor. This, in turn, expands the potential applications of solitons in fields such as fiber optic communications, quantum field theory, and fluid dynamics.

This study explores the impact of multiplicative white noise on the perturbed generalized CLL equation, analyzed within the framework of Itô calculus. The incorporation of multiplicative white noise introduces stochastic perturbations that significantly alter the dynamics of the system. The modified structure of the perturbed generalized CLL equation, reflecting the influence of this stochastic noise, is expressed as follows:

$$iq_t + aq_{xx} + bq_{xt} + ic |q|^{2n} q_x + \sigma (q - ibq_x) \frac{dW(t)}{dt} + i\left\{ \alpha q_x + \lambda \left(|q|^{2n} q\right)_x + \beta \left(|q|^{2n}\right)_x q \right\} = 0. \quad (1)$$

The complex-valued function $q = q(x, t)$ describes the wave profile, encapsulating the essential characteristics of the wave's behavior over space and time. The coefficients a, b, and c play critical roles, representing the effects of chromatic dispersion, spatiotemporal dispersion, and nonlinear dispersion, respectively. These coefficients govern the evolution of the wave and dictate how various dispersion phenomena influence its shape and dynamics. The parameter α is specifically associated with inter-modal dispersion, capturing the interactions between different modes within the medium. Meanwhile, λ is a key parameter that characterizes the self-steepening effect observed in short pulses, a phenomenon where the pulse shape becomes increasingly asymmetric as it propagates. Additionally, the coefficient β is tied to nonlinear dispersion, further contributing to the complex interplay between the wave's nonlinear and dispersive properties. The noise level within the system is quantified by the parameter σ, which introduces stochastic fluctuations into the model through the use of $W(t)$, a standard Wiener process. The Wiener process, often referred to as Brownian motion, is a fundamental concept in stochastic processes. It is defined by its initial condition $W(0) = 0$, and for any $0 \le s < t$, the increment $W(t) - W(s)$ follows a normal distribution with a mean of zero and a variance proportional to $t - s$ ($W(t) - W(s) \sim N(0, t - s)$). This implies that the process has independent increments, meaning that for any sequence $0 \le t_1 < t_2 < \cdots < t_n$, the increments $W(t_2) - W(t_1)$, $W(t_3) - W(t_2)$, ..., $W(t_n) - W(t_{n-1})$ are mutually independent. A notable feature of the Wiener process is its continuous trajectory, ensuring that the noise introduced into the system evolves smoothly over time. The magnitude of the noise can be controlled through the derivative of $W(t)$ with respect to time, denoted by $\frac{dW}{dt}$. This derivative represents the instantaneous rate of change of the Wiener process, allowing for precise modulation of the noise's impact on the wave profile. As highlighted in several studies [22–24], these stochastic components are essential for modeling real-world scenarios where noise and randomness play significant roles in the dynamics of wave propagation.

The study unfolds with a systematic exploration of the methodologies and results, structured across five key sections to ensure clarity and logical progression. In the second section, the study introduces the improved extended tanh-function method, delving into its mathematical foundations and operational mechanics. This advanced analytical tool builds upon the conventional tanh-function method, incorporating enhancements that allow for the efficient handling of nonlinear differential equations, especially in the presence of complex terms such as stochastic perturbations. Detailed

explanations are provided to showcase how this method facilitates the derivation of exact solutions with improved accuracy and generality. Illustrative examples and step-by-step derivations demonstrate its robustness and adaptability, emphasizing its suitability for analyzing the stochastic generalized CLL equation. The third section transitions to a critical step in the analysis: the introduction of a wave transformation scheme designed to incorporate the effects of white noise. This transformation is pivotal as it enables the conversion of the stochastic partial differential equation into a nonlinear ordinary differential equation (ODE). The section outlines the mathematical rationale behind the transformation, explaining how the inclusion of white noise, modeled in the Itô sense, impacts the governing dynamics. By simplifying the problem to an ODE form, the study creates a framework that makes the system more tractable for soliton analysis while retaining the essential influence of stochastic perturbations. The technical details of the transformation are meticulously discussed, highlighting its role in bridging the stochastic and deterministic aspects of the governing equation. The fourth section forms the core of the study, where the focus shifts to a comprehensive investigation of how white noise influences the soliton dynamics of the governing model. Through an extensive set of visual representations, including Figures 1–40, this section explores the intricate interplay between noise, nonlinearity, and soliton structures. The figures are categorized and analyzed in detail, depicting a variety of soliton solutions such as singular, bright, and dark solitons under different parameter settings. Each figure is accompanied by an explanation of the underlying physics and the role of white noise in shaping the observed dynamics. For instance, surface plots illustrate the three-dimensional evolution of solitons, contour plots reveal phase variations, and 2D slices highlight temporal and spatial profiles. This section underscores the critical insights gained from the visual analysis, showing how noise intensity and system parameters influence soliton stability, amplitude, and propagation characteristics. Finally, the fifth section serves as a concluding summary, synthesizing the findings of the study and reflecting on their broader implications. It recapitulates the key contributions, emphasizing the novel formulation of the stochastic generalized CLL equation and the diversity of soliton solutions uncovered through the improved extended tanh-function method. The implications of these findings are discussed in the context of nonlinear optics, with a particular focus on their potential applications in optical communication, signal processing, and interdisciplinary research. The section also outlines avenues for future exploration, suggesting that further studies could expand on the current work by examining higher-dimensional systems, alternative forms of stochastic perturbations, and experimental validation of the theoretical results.

By systematically progressing through these sections, the study ensures a cohesive narrative that integrates methodological innovation, rigorous analysis, and insightful interpretations, laying a robust foundation for future advancements in the field.

2. The improved extended tanh-function methodology

In our analysis, we initiate by exploring the methodology through an examination of a primary stochastic model characterized by the structure:

$$G(u, u_x, u_t, u_{xt}, u_{xx}, ...) + \sigma u \frac{dW(t)}{dt} = 0, \tag{2}$$

wherein $u = u(x, t)$ expresses the wave solution, and t and x sequentially denote the temporal and spatial dimensions.

Applying the change of variables

$$u(x,t) = U(\xi)e^{(\sigma W(t) - \sigma^2 t)}, \xi = \mu(x - \upsilon t), \tag{3}$$

allows Eq (3) to be rewritten as the following ODE:

$$P(U, -\mu\upsilon U', \mu U', \mu^2 U'', ...) = 0, \tag{4}$$

with μ referring to the wave width, ξ representing the new wave variable, and υ specifying the wave velocity.

Step 1: Equation (4) is proposed to be of the form:

$$U(\xi) = \eta_0 + \sum_{i=1}^{N} \left\{ \eta_i \phi(\xi)^i + \mu_i \phi(\xi)^{-i} \right\}, \tag{5}$$

with

$$\phi'(\xi)^2 = \sum_{l=0}^{4} \tau_l \phi(\xi)^l, \tag{6}$$

which results in a comprehensive set of solutions [25].

Case 1: $\tau_0 = \tau_1 = \tau_3 = 0$.

Bright and singular solitons are sequentially derived as follows:

$$\phi(\xi) = \sqrt{-\frac{\tau_2}{\tau_4}} \operatorname{sech}\left[\sqrt{\tau_2}\,\xi \right], \quad \tau_2 > 0, \ \tau_4 < 0, \tag{7}$$

and

$$\phi(\xi) = \sqrt{\frac{\tau_2}{\tau_4}} \operatorname{csch}\left[\sqrt{\tau_2}\,\xi \right], \quad \tau_2 > 0, \ \tau_4 > 0. \tag{8}$$

Case 2: $\tau_0 = \frac{\tau_2^2}{4\tau_4}$, $\tau_1 = \tau_3 = 0$.

Dark and singular solitons are achieved as follows:

$$\phi(\xi) = \sqrt{-\frac{\tau_2}{2\tau_4}} \tanh\left[\sqrt{-\frac{\tau_2}{2}}\,\xi \right], \quad \tau_2 < 0, \ \tau_4 > 0, \tag{9}$$

and

$$\phi(\xi) = \sqrt{-\frac{\tau_2}{2\tau_4}} \coth\left[\sqrt{-\frac{\tau_2}{2}}\,\xi \right], \quad \tau_2 < 0, \ \tau_4 > 0. \tag{10}$$

Case 3: $\tau_2 = \tau_4 = 0$, $\tau_0 \neq 0$, $\tau_1 \neq 0$, $\tau_3 > 0$.

Thus, Eq (6) holds the Weierstrass elliptic function (WEF):

$$\phi(\xi) = \wp\left(\frac{\sqrt{\tau_3}}{2}\xi, g_2, g_3 \right), \tag{11}$$

where $g_2 = -\frac{4\tau_1}{\tau_3}$ and $g_3 = -\frac{4\tau_0}{\tau_3}$ are referred to as invariants of the WEF.

Case 4: $\tau_0 = \frac{\tau_1^2}{4\tau_2}$, $\tau_3 = \tau_4 = 0$.

An exponential-type solution is obtained:

$$\phi(\xi) = -\frac{\tau_1}{2\tau_2} + \exp\left[\varepsilon \sqrt{\tau_2}\,\xi\right], \quad \tau_2 > 0. \tag{12}$$

Case 5: $\tau_0 = \tau_3 = \tau_4 = 0$.

A solitary wave solution is obtained:

$$\phi(\xi) = \pm \sqrt{\frac{\tau_0}{\tau_2}} \sinh\left[\sqrt{-\tau_2}\,\xi\right], \quad \tau_0 > 0, \ \tau_2 > 0. \tag{13}$$

Case 6: $\tau_0 = \tau_1 = 0, \ \tau_2, \ \tau_4 > 0, \ \tau_3 \neq \pm 2\sqrt{\tau_2\tau_4}$.

Bright-dark and singular-singular solitons are retrieved as follows:

$$\phi(\xi) = \frac{-\tau_2 \mathrm{sech}^2\left[\frac{1}{2}\sqrt{\tau_2}\,\xi\right]}{\pm 2\sqrt{\tau_2\tau_4}\,\tanh\left[\frac{1}{2}\sqrt{\tau_2}\,\xi\right] + \tau_3}, \tag{14}$$

and

$$\phi(\xi) = \frac{\tau_2 \mathrm{csch}^2\left[\frac{1}{2}\sqrt{\tau_2}\,\xi\right]}{\pm 2\sqrt{\tau_2\tau_4}\,\coth\left[\frac{1}{2}\sqrt{\tau_2}\,\xi\right] + \tau_3}. \tag{15}$$

Step 2: The determination of the positive integer N in Eq (5) is carried out by balancing the highest-order derivatives with the nonlinear terms in Eq (4).

Step 3: When Eq (5) along with (6) are substituted into Eq (4), the resulting system takes the form of a polynomial in ϕ. By grouping terms by their respective powers of ϕ and equating each group to zero, an over-determined algebraic system is obtained. Solving this system determines the unknown parameters, leading to the solutions of Eq (2).

3. New solitary waveforms

We employ a particular solution format, as outlined below, to solve Eq (1):

$$q(x, t) = U(\xi)\, e^{i(-\kappa x + \omega t + \sigma W(t) - \sigma^2 t + \theta_0)}, \tag{16}$$

where the definition of the wave parameter ξ is

$$\xi = k(x - vt). \tag{17}$$

The function $U(\xi)$ plays a crucial role in describing the soliton dynamics, as it represents the real-valued amplitude of the soliton solution, which is a measure of the soliton's height or strength as it propagates through the medium. The parameter v is the soliton's propagation velocity, indicating the rate at which the soliton travels along the spatial coordinate. This velocity plays a significant role in understanding the stability and dynamics of the soliton as it interacts with the medium. The parameter κ is identified as the soliton's frequency, which determines the oscillatory nature of the soliton's profile and is closely related to its temporal evolution. Similarly, k defines the wave's width, which provides insight into the soliton's spatial spread or localization. A smaller k corresponds to a

more localized soliton, while a larger k leads to a broader soliton profile. The parameter ω, referred to as the wave number, governs the spatial periodicity of the soliton, linking it to the underlying wave structure of the solution. Another key parameter, σ, represents the noise intensity, which captures the stochastic effects that influence the soliton's behavior in the presence of multiplicative white noise. This parameter is particularly important in exploring the stability and robustness of soliton solutions under random perturbations. The phase constant θ_0 determines the initial phase of the soliton. By substituting the proposed solution from Eq (16) into the governing model, Eq (1), the relationship between these parameters is established, and a rigorous mathematical framework is developed. This substitution reduces the governing equation to a simpler form, allowing us to isolate the contributions of the real-valued amplitude $U(\xi)$ and other parameters. The process leads to the derivation of a critical expression that captures the essence of the soliton solution. The result highlights the real part of the solution, which is given as:

$$(a - bv)U'' + U\left(-a\kappa^2 + \alpha\kappa - (b\kappa - 1)\left(\sigma^2 - \omega\right)\right) + \kappa(c + \lambda)U^{2n+1} = 0, \tag{18}$$

and the imaginary part is:

$$U'\left(-2a\kappa + \alpha + b\kappa v - b\sigma^2 + b\omega + (c + \lambda + 2n(\beta + \lambda))U^{2n} - v\right) = 0. \tag{19}$$

This expression provides valuable insights into the soliton's characteristics, shedding light on how the amplitude, frequency, wave number, width, and noise intensity collectively shape the soliton's dynamics.

From the imaginary part (19), we can derive the soliton speed

$$v = \frac{2a\kappa - \alpha + b\sigma^2 - b\omega}{b\kappa - 1}, \tag{20}$$

with the constraint

$$c + \lambda + 2n(\beta + \lambda) = 0. \tag{21}$$

In our discussion, we will examine the formula given by (18) under the specific constraints outlined in (20). To obtain a positive integer balance number N, we will conduct this analysis through the application of a transformation:

$$U(\xi) = V(\xi)^{\frac{1}{n}}, \tag{22}$$

which transforms Eq (18) to

$$n^2 V^2 \left(-a\kappa^2 + \alpha\kappa - (b\kappa - 1)\left(\sigma^2 - \omega\right)\right) + nV(a - bv)V''$$
$$-(n - 1)(a - bv)V'^2 + \kappa n^2(c + \lambda)V^4 = 0. \tag{23}$$

We present a comprehensive description of the proposed technique, outlining an auxiliary equation that includes various solutions of diverse nature. The present study investigates the ability of these particular types to recover singular, dark, and bright solitons successfully.

According to Step 2 in Section 2, we need to determine the positive integer N by balancing the highest derivative with the nonlinear terms in Eq (23). The highest derivative in this context is V'', while the nonlinear terms include V^2, V'^2, and V^4. By balancing VV'' (which contributes $N + N + 2$) with V^4 (which contributes $4N$) in Eq (23), we obtain $N = 1$. Similarly, by balancing V'^2 (which

contributes $2(N + 1)$) with V^4 (which contributes $4N$) in Eq (23), we again find that $N = 1$. Since N must be the positive integer satisfying these conditions, we conclude that $N = 1$. Consequently, the solution can be expressed as follows:

$$V(\xi) = \eta_0 + \eta_1 \phi(\xi) + \frac{\mu_1}{\phi(\xi)}. \tag{24}$$

Inserting both Eqs (24) and (6) into Eq (23) leads to algebraic equations. The solutions to this system are given by:

Case 1: For $\tau_0 = \tau_1 = \tau_3 = 0$:

$$\eta_0 = 0, \ \mu_1 = 0, \ \tau_2 = \frac{n^2 \left(a\kappa^2 - \alpha\kappa + b\kappa\sigma^2 - b\kappa\omega - \sigma^2 + \omega\right)}{a - bv}, \ \tau_4 = -\frac{\eta_1^2 \kappa n^2 (c + \lambda)}{(n + 1)(a - bv)}. \tag{25}$$

The analysis yields the solutions to Eq (1):

$$q(x, t) = \left\{ \sqrt{\frac{(n + 1)\left(a\kappa^2 - \alpha\kappa + b\kappa\sigma^2 - b\kappa\omega - \sigma^2 + \omega\right)}{\kappa(c + \lambda)}} \right.$$
$$\left. \times \text{sech}\left[\sqrt{\frac{n^2 \left(a\kappa^2 - \alpha\kappa + b\kappa\sigma^2 - b\kappa\omega - \sigma^2 + \omega\right)}{a - bv}}(x - vt)\right] \right\}^{\frac{1}{n}}$$
$$\times e^{i\left(-\kappa x + \omega t - \sigma^2 t + \sigma w(t) + \theta_0\right)}, \tag{26}$$

and

$$q(x, t) = \left\{ \sqrt{\frac{(n + 1)\left(a\kappa^2 - \alpha\kappa + b\kappa\sigma^2 - b\kappa\omega - \sigma^2 + \omega\right)}{\kappa(c + \lambda)}} \right.$$
$$\left. \times \text{csch}\left[\sqrt{\frac{n^2 \left(a\kappa^2 - \alpha\kappa + b\kappa\sigma^2 - b\kappa\omega - \sigma^2 + \omega\right)}{a - bv}}(x - vt)\right] \right\}^{\frac{1}{n}}$$
$$\times e^{i\left(-\kappa x + \omega t - \sigma^2 t + \sigma w(t) + \theta_0\right)}. \tag{27}$$

Case 2: For $\tau_0 = \frac{\tau_2^2}{4\tau_4}$, $\tau_1 = \tau_3 = 0$:
Result 1:

$$\eta_0 = 0, \ \eta_1 = -\frac{(n + 1)\left(-a\kappa^2 + \alpha\kappa - b\kappa\sigma^2 + b\kappa\omega + \sigma^2 - \omega\right)}{4\kappa\mu_1(c + \lambda)},$$
$$\tau_2 = -\frac{n^2 \left(a\kappa^2 - \alpha\kappa + b\kappa\sigma^2 - b\kappa\omega - \sigma^2 + \omega\right)}{2(a - bv)},$$
$$\tau_4 = -\frac{n^2(n + 1)\left(-a\kappa^2 + \alpha\kappa - b\kappa\sigma^2 + b\kappa\omega + \sigma^2 - \omega\right)^2}{16\kappa\mu_1^2(c + \lambda)(a - bv)}. \tag{28}$$

The derived solutions for Eq (1) are presented below:

$$q(x,t) = \left\{ \pm \sqrt{\frac{(n+1)\left(-a\kappa^2 + \alpha\kappa - b\kappa\sigma^2 + b\kappa\omega + \sigma^2 - \omega\right)}{\kappa(c+\lambda)}} \right.$$

$$\times \text{csch}\left[\sqrt{\frac{n^2\left(a\kappa^2 - \alpha\kappa + b\kappa\sigma^2 - b\kappa\omega - \sigma^2 + \omega\right)}{a-bv}}(x-vt)\right]\right\}^{\frac{1}{n}}$$

$$\times e^{i\left(-\kappa x + \omega t - \sigma^2 t + \sigma w(t) + \theta_0\right)}. \tag{29}$$

Result 2:

$$\eta_0 = \pm \frac{\sqrt{a\kappa^2 - \alpha\kappa + (b\kappa - 1)\left(\sigma^2 - \omega\right)}}{2\sqrt{\kappa(c+\lambda)}}, \; \eta_1 = 0,$$

$$\tau_2 = -\frac{2\left(a\kappa^2 - \alpha\kappa + (b\kappa - 1)\left(\sigma^2 - \omega\right)\right)}{a-bv},$$

$$\tau_4 = \frac{\left(a\kappa^2 - \alpha\kappa + (b\kappa - 1)\left(\sigma^2 - \omega\right)\right)^2}{4\kappa\mu_1^2(c+\lambda)(a-bv)}, \; n = -2. \tag{30}$$

The resulting solutions to Eq (1) are as follows:

$$q(x,t) = \left\{ \frac{\sqrt{a\kappa^2 - \alpha\kappa + (b\kappa - 1)\left(\sigma^2 - \omega\right)}}{2\sqrt{\kappa(c+\lambda)}}\left(\coth\left[\sqrt{\frac{a\kappa^2 - \alpha\kappa + (b\kappa - 1)\left(\sigma^2 - \omega\right)}{a-bv}}(x-vt)\right] \pm 1\right)\right\}^{-\frac{1}{2}}$$

$$\times \; e^{i\left(-\kappa x + \omega t - \sigma^2 t + \sigma w(t) + \theta_0\right)}, \tag{31}$$

and

$$q(x,t) = \left\{ \frac{\sqrt{a\kappa^2 - \alpha\kappa + (b\kappa - 1)\left(\sigma^2 - \omega\right)}}{2\sqrt{\kappa(c+\lambda)}}\left(\tanh\left[\sqrt{\frac{a\kappa^2 - \alpha\kappa + (b\kappa - 1)\left(\sigma^2 - \omega\right)}{a-bv}}(x-vt)\right] \pm 1\right)\right\}^{-\frac{1}{2}}$$

$$\times \; e^{i\left(-\kappa x + \omega t - \sigma^2 t + \sigma w(t) + \theta_0\right)}. \tag{32}$$

Result 3:

$$\eta_0 = 0, \; \eta_1 = 0, \; \tau_2 = \frac{a\kappa^2 - \alpha\kappa + (b\kappa - 1)\left(\sigma^2 - \omega\right)}{a-bv},$$

$$\tau_4 = -\frac{\left(a\kappa^2 - \alpha\kappa + (b\kappa - 1)\left(\sigma^2 - \omega\right)\right)^2}{2\kappa\mu_1^2(c+\lambda)(a-bv)}, \; n = 1. \tag{33}$$

Accordingly, the solutions to Eq (1) can be expressed as follows:

$$q(x,t) = \left\{ \sqrt{\frac{a\kappa^2 - \alpha\kappa + (b\kappa - 1)\left(\sigma^2 - \omega\right)}{\kappa(c+\lambda)}} \coth\left[\sqrt{-\frac{a\kappa^2 - \alpha\kappa + (b\kappa - 1)\left(\sigma^2 - \omega\right)}{2(a-bv)}}(x-vt)\right]\right\}$$

$$\times \quad e^{i\left(-\kappa x+\omega t-\sigma^2 t+\sigma w(t)+\theta_0\right)}, \tag{34}$$

and

$$
\begin{aligned}
q(x,t) &= \left\{ \sqrt{\frac{a\kappa^2 - \alpha\kappa + (b\kappa - 1)\left(\sigma^2 - \omega\right)}{\kappa(c + \lambda)}} \tanh\left[\sqrt{-\frac{a\kappa^2 - \alpha\kappa + (b\kappa - 1)\left(\sigma^2 - \omega\right)}{2(a - bv)}}(x - vt)\right] \right\} \\
&\times \quad e^{i\left(-\kappa x+\omega t-\sigma^2 t+\sigma w(t)+\theta_0\right)}.
\end{aligned}
\tag{35}
$$

Case 3: For $\tau_1 = \tau_3 = \tau_4 = 0$:

$$\eta_0 = 0, \ \eta_1 = 0, \ \tau_0 = -\frac{\kappa\mu_1^2 n^2(c + \lambda)}{(n + 1)(a - bv)}, \ \tau_2 = \frac{n^2\left(a\kappa^2 - \alpha\kappa + b\kappa\sigma^2 - b\kappa\omega - \sigma^2 + \omega\right)}{a - bv}. \tag{36}$$

Accordingly, the solutions for Eq (1) are found:

$$
\begin{aligned}
q(x,t) &= \left\{ \pm \sqrt{-\frac{(n + 1)\left(a\kappa^2 - \alpha\kappa + b\kappa\sigma^2 - b\kappa\omega - \sigma^2 + \omega\right)}{\kappa(c + \lambda)}} \right. \\
&\quad \left. \times \mathrm{csch}\left[\sqrt{-\frac{n^2\left(a\kappa^2 - \alpha\kappa + b\kappa\sigma^2 - b\kappa\omega - \sigma^2 + \omega\right)}{a - bv}}(x - vt)\right] \right\}^{\frac{1}{n}} \\
&\times \quad e^{i\left(-\kappa x+\omega t-\sigma^2 t+\sigma w(t)+\theta_0\right)}.
\end{aligned}
\tag{37}
$$

Case 4: For $\tau_0 = \tau_1 = 0$:
Result 1:

$$\eta_0 = 0, \ \mu_1 = 0, \ \tau_2 = \frac{n^2\left(a\kappa^2 - \alpha\kappa + (b\kappa - 1)\left(\sigma^2 - \omega\right)\right)}{a - bv}, \ \tau_3 = 0, \ \tau_4 = -\frac{\eta_1^2\kappa n^2(c + \lambda)}{(n + 1)(a - bv)}. \tag{38}$$

As a result, Eq (1) yields the following solutions:

$$
\begin{aligned}
q(x,t) &= \left\{ \pm \sqrt{-\frac{(n + 1)\left(a\kappa^2 - \alpha\kappa + (b\kappa - 1)\left(\sigma^2 - \omega\right)\right)}{\kappa(c + \lambda)}} \right. \\
&\quad \left. \times \mathrm{csch}\left[\sqrt{\frac{n^2\left(a\kappa^2 - \alpha\kappa + (b\kappa - 1)\left(\sigma^2 - \omega\right)\right)}{a - bv}}(x - vt)\right] \right\}^{\frac{1}{n}} \\
&\times e^{i\left(-\kappa x+\omega t-\sigma^2 t+\sigma w(t)+\theta_0\right)}.
\end{aligned}
\tag{39}
$$

Result 2:

$$
\begin{aligned}
\eta_0 &= \pm\frac{\sqrt{a\kappa^2 - \alpha\kappa + (b\kappa - 1)\left(\sigma^2 - \omega\right)}}{\sqrt{\kappa(c + \lambda)}}, \ \mu_1 = 0, \ \tau_2 = -\frac{4\left(a\kappa^2 - \alpha\kappa + (b\kappa - 1)\left(\sigma^2 - \omega\right)\right)}{a - bv}, \\
\tau_3 &= \mp\frac{16\eta_1\sqrt{\kappa(c + \lambda)}\sqrt{a\kappa^2 - \alpha\kappa + (b\kappa - 1)\left(\sigma^2 - \omega\right)}}{3(a - bv)}, \ \tau_4 = -\frac{4\eta_1^2\kappa(c + \lambda)}{3(a - bv)}, \ n = 2.
\end{aligned}
\tag{40}
$$

Following this, Eq (1) provides the following solutions:

$$
\begin{aligned}
q(x,t) &= \left\{ \left(\pm \frac{\sqrt{a\kappa^2 - \alpha\kappa + (b\kappa - 1)\left(\sigma^2 - \omega\right)}}{\sqrt{\kappa(c + \lambda)}} \left(\frac{\operatorname{sech}^2\left[\sqrt{-\frac{a\kappa^2 - \alpha\kappa + (b\kappa-1)\left(\sigma^2 - \omega\right)}{a - bv}}(x - vt)\right]}{\frac{2}{\sqrt{3}}\tanh\left[\sqrt{-\frac{a\kappa^2 - \alpha\kappa + (b\kappa-1)\left(\sigma^2 - \omega\right)}{a - bv}}(x - vt)\right] - \frac{4}{3}} + 1 \right)\right)^{\frac{1}{2}} \right\} \\
&\times\ e^{i\left(-\kappa x + \omega t - \sigma^2 t + \sigma w(t) + \theta_0\right)},
\end{aligned}
\tag{41}
$$

and

$$
\begin{aligned}
q(x,t) &= \left\{ \left(\pm \frac{\sqrt{a\kappa^2 - \alpha\kappa + (b\kappa - 1)\left(\sigma^2 - \omega\right)}}{\sqrt{\kappa(c + \lambda)}} \left(\frac{\operatorname{csch}^2\left[\sqrt{-\frac{a\kappa^2 - \alpha\kappa + (b\kappa-1)\left(\sigma^2 - \omega\right)}{a - bv}}(x - vt)\right]}{\frac{2}{\sqrt{3}}\coth\left[\sqrt{-\frac{a\kappa^2 - \alpha\kappa + (b\kappa-1)\left(\sigma^2 - \omega\right)}{a - bv}}(x - vt)\right] - \frac{4}{3}} + 1 \right)\right)^{\frac{1}{2}} \right\} \\
&\times\ e^{i\left(-\kappa x + \omega t - \sigma^2 t + \sigma w(t) + \theta_0\right)}.
\end{aligned}
\tag{42}
$$

Result 3:

$$
\eta_0 = \mp \frac{\sqrt{a\kappa^2 - \alpha\kappa + (b\kappa - 1)\left(\sigma^2 - \omega\right)}}{\sqrt{\kappa(c + \lambda)}},\ \mu_1 = 0,\ \tau_2 = -\frac{2\left(a\kappa^2 - \alpha\kappa + (b\kappa - 1)\left(\sigma^2 - \omega\right)\right)}{a - bv},
$$

$$
\tau_3 = \pm \frac{2\eta_1\sqrt{\kappa(c + \lambda)}\sqrt{a\kappa^2 - \alpha\kappa + (b\kappa - 1)\left(\sigma^2 - \omega\right)}}{a - bv},\ \tau_4 = -\frac{\eta_1^2\kappa(c + \lambda)}{2(a - bv)},\ n = 1.
\tag{43}
$$

This leads to the derivation of the solutions for Eq (1):

$$
\begin{aligned}
q(x,t) &= \pm \frac{\sqrt{a\kappa^2 - \alpha\kappa + (b\kappa - 1)\left(\sigma^2 - \omega\right)}}{\sqrt{\kappa(c + \lambda)}}\left(\frac{\operatorname{sech}^2\left[\sqrt{-\frac{a\kappa^2 - \alpha\kappa + (b\kappa-1)\left(\sigma^2 - \omega\right)}{2(a - bv)}}(x - vt)\right]}{\tanh\left[\sqrt{-\frac{a\kappa^2 - \alpha\kappa + (b\kappa-1)\left(\sigma^2 - \omega\right)}{2(a - bv)}}(x - vt)\right] + 1} - 1 \right) \\
&\times\ e^{i\left(-\kappa x + \omega t - \sigma^2 t + \sigma w(t) + \theta_0\right)},
\end{aligned}
\tag{44}
$$

and

$$
\begin{aligned}
q(x,t) &= \pm \frac{\sqrt{a\kappa^2 - \alpha\kappa + (b\kappa - 1)\left(\sigma^2 - \omega\right)}}{\sqrt{\kappa(c + \lambda)}}\left(\frac{\operatorname{csch}^2\left[\sqrt{-\frac{a\kappa^2 - \alpha\kappa + (b\kappa-1)\left(\sigma^2 - \omega\right)}{2(a - bv)}}(x - vt)\right]}{\coth\left[\sqrt{-\frac{a\kappa^2 - \alpha\kappa + (b\kappa-1)\left(\sigma^2 - \omega\right)}{2(a - bv)}}(x - vt)\right] + 1} + 1 \right) \\
&\times\ e^{i\left(-\kappa x + \omega t - \sigma^2 t + \sigma w(t) + \theta_0\right)}.
\end{aligned}
\tag{45}
$$

Result 4:

$$
\eta_0 = \mp \frac{\sqrt{a\kappa^2 - \alpha\kappa + (b\kappa - 1)\left(\sigma^2 - \omega\right)}}{\sqrt{\kappa(c + \lambda)}},\ \mu_1 = 0,\ \tau_2 = \frac{4\left(a\kappa^2 - \alpha\kappa + (b\kappa - 1)\left(\sigma^2 - \omega\right)\right)}{a - bv},
$$

$$\tau_3 = \pm \frac{8\eta_1 \sqrt{\kappa(c+\lambda)} \sqrt{a\kappa^2 - \alpha\kappa + (b\kappa - 1)(\sigma^2 - \omega)}}{a - bv}, \quad \tau_4 = \frac{4\eta_1^2 \kappa(c+\lambda)}{a - bv}, \quad n = -2. \tag{46}$$

The analysis yields the solutions to Eq (1):

$$q(x,t) = \left\{ \mp \frac{\sqrt{a\kappa^2 - \alpha\kappa + (b\kappa - 1)(\sigma^2 - \omega)}}{\sqrt{\kappa(c+\lambda)}} \left(\frac{\operatorname{sech}^2\left[\sqrt{\frac{a\kappa^2 - \alpha\kappa + (b\kappa - 1)(\sigma^2 - \omega)}{a - bv}}(x - vt)\right]}{2\left(\tanh\left[\sqrt{\frac{a\kappa^2 - \alpha\kappa + (b\kappa - 1)(\sigma^2 - \omega)}{a - bv}}(x - vt)\right] + 1\right)} + 1 \right) \right\}^{-\frac{1}{2}}$$
$$\times \ e^{i\left(-\kappa x + \omega t - \sigma^2 t + \sigma w(t) + \theta_0\right)}, \tag{47}$$

and

$$q(x,t) = \left\{ \mp \frac{\sqrt{a\kappa^2 - \alpha\kappa + (b\kappa - 1)(\sigma^2 - \omega)}}{\sqrt{\kappa(c+\lambda)}} \left(\frac{\operatorname{csch}^2\left[\sqrt{\frac{a\kappa^2 - \alpha\kappa + (b\kappa - 1)(\sigma^2 - \omega)}{a - bv}}(x - vt)\right]}{2\left(\coth\left[\sqrt{\frac{a\kappa^2 - \alpha\kappa + (b\kappa - 1)(\sigma^2 - \omega)}{a - bv}}(x - vt)\right] + 1\right)} + 1 \right) \right\}^{-\frac{1}{2}}$$
$$\times \ e^{i\left(-\kappa x + \omega t - \sigma^2 t + \sigma w(t) + \theta_0\right)}. \tag{48}$$

4. Results and discussion

This section discusses the results obtained from the analysis of various types of optical solitons, including bright, dark, singular, straddled singular-singular, and straddled bright-dark solitons, as depicted in Figures 1–40. Each figure set corresponds to a specific soliton type and explores the influence of key parameters such as time evolution, multiplicative white noise, and power nonlinearity. The figures also investigate the soliton dynamics through surface plots, contour plots, and 2D plots, providing a comprehensive view of their behavior under varying conditions. In Figures 1–40, we set the parameters: $b = 1.2$, $\kappa = 1$, $a = 1$, $\alpha = 1.8$, $\omega = 0.8$, $\theta_0 = 1$, $c = 1.3$, and $\lambda = 2$.

Figure 1 addresses the bright soliton $q(x,t)$ described by the complex-valued solution (26) without the effect of multiplicative white noise ($\sigma = 0$). This figure presents nine subfigures focusing on the modulus, real part, and imaginary part of the soliton. The surface plot, contour plot, and 2D plot reveal that the bright soliton maintains a stable, localized shape as time evolves, showing a peak amplitude that is consistent across different time slices.

Figures 2–6 introduce the effect of increasing multiplicative white noise ($\sigma = 2$ to $\sigma = 6$). These figures highlight the gradual broadening and deformation of the soliton's profile as noise intensity increases. Surface plots indicate that higher noise levels disrupt the soliton's localized nature, leading to a more dispersed structure. This behavior is also evident in the contour and 2D plots, where the soliton's peak diminishes, and the surrounding wave structure becomes more irregular.

Figures 37 and 38 explore the influence of the power nonlinearity parameter n on the bright soliton both with and without noise. Figure 37 shows that as n increases (from $n = 3$ to $n = 5$), the soliton's peak becomes sharper, and its width decreases, indicating stronger confinement. Figure 38 demonstrates that under the influence of noise ($\sigma = 1$ to $\sigma = 6$), the soliton's structure deteriorates more rapidly with higher n, suggesting a heightened sensitivity to noise when the nonlinearity is

stronger. Bright solitons exhibit robust stability in the absence of noise, characterized by a well-defined peak and a localized waveform. The introduction of multiplicative white noise disrupts this stability, leading to the broadening and eventual dispersion of the soliton. Additionally, stronger power nonlinearity enhances the soliton's confinement but also increases its vulnerability to noise-induced perturbations.

Figure 7 examines the singular soliton $q(x, t)$ described by the complex-valued solution (27) without noise ($\sigma = 0$). The modulus, real part, and imaginary part reveal that singular solitons have a distinctive sharp peak and a steep gradient, with the wave structure rapidly approaching zero outside the soliton core. The surface and contour plots confirm the highly localized and singular nature of these solitons.

Figures 8–12 assess the impact of increasing noise ($\sigma = 2$ to $\sigma = 6$) on the singular soliton. The results show that singular solitons are particularly sensitive to noise, with even moderate noise levels ($\sigma = 2$) leading to significant deformation. Higher noise intensities cause the soliton's peak to flatten and the gradient to become less steep, indicating a loss of the soliton's singular characteristics.

Figures 39 and 40 investigate the role of power nonlinearity n on the singular soliton, both with and without noise. Figure 39 shows that increasing n sharpens the soliton's peak and intensifies its singularity. Figure 40 illustrates that under noise, the soliton's peak becomes increasingly disrupted as n rises, with the singular structure breaking down more rapidly, similar to the observations made for bright solitons. Singular solitons are highly localized and characterized by sharp peaks and steep gradients. They are, however, more susceptible to noise compared to bright solitons, with even small amounts of noise leading to significant structural degradation. Increasing the power nonlinearity sharpens the singularity but also heightens the soliton's sensitivity to noise.

Figure 13 presents the dark soliton $q(x, t)$ described by the complex-valued solution (32) without noise ($\sigma = 0$). Unlike bright and singular solitons, dark solitons are characterized by a localized dip in the wave intensity rather than a peak. The surface and contour plots show that the soliton maintains a consistent trough depth and width over time, suggesting stable propagation.

Figures 14–18 explore the effects of increasing noise ($\sigma = 2$ to $\sigma = 6$) on dark solitons. As noise intensity increases, the soliton's trough becomes less defined, and the surrounding wave structure becomes more turbulent. The 2D plots show that the soliton's depth decreases, and the trough becomes wider, indicating a partial loss of the soliton's dark characteristics. Dark solitons are stable in the absence of noise, maintaining a well-defined trough that propagates without significant change. However, the introduction of noise disrupts this stability, leading to a shallower and broader trough. This suggests that dark solitons are less robust against noise compared to bright solitons but more stable than singular solitons.

Figure 19 illustrates the behavior of the singular soliton $q(x, t)$ as described by the complex-valued solution (31) in the absence of noise ($\sigma = 0$). The figure presents the modulus, real part, and imaginary part of the singular soliton. These plots demonstrate that singular solitons exhibit a highly distinctive sharp peak and a steep gradient. The wave structure of the soliton rapidly decays to near zero outside its core, underscoring its highly localized and singular nature. The surface and contour plots further reinforce this observation, showing the soliton's localized nature and the pronounced singularity at its peak.

Figures 20–24 explore the effects of increasing noise levels, ranging from $\sigma = 2$ to $\sigma = 6$, on the singular soliton. The analysis reveals that singular solitons are particularly sensitive to the introduction of noise. Even at moderate noise levels ($\sigma = 2$), the soliton undergoes substantial

deformation. As the noise intensity increases, the peak of the soliton becomes progressively flattened, and the gradient of the soliton becomes less steep. This flattening effect indicates a significant degradation of the soliton's singular characteristics. Higher noise levels exacerbate this effect, leading to a notable loss of the soliton's distinctive sharp peak and steep gradient. Singular solitons are characterized by their highly localized nature, sharp peaks, and steep gradients. However, they exhibit a pronounced sensitivity to noise compared to bright solitons. Even small amounts of noise can significantly compromise the structural integrity of singular solitons. Furthermore, increasing the power nonlinearity sharpens the singularity of the soliton but also amplifies its sensitivity to noise, resulting in greater structural degradation with increasing noise intensity.

Figures 25–30 address the straddled bright-dark soliton $q(x, t)$ described by the complex-valued solution (41). These solitons exhibit a combination of bright and dark soliton characteristics, with a localized peak (bright) adjacent to a localized trough (dark). The surface and contour plots reveal a complex structure where the bright and dark components maintain their respective identities but are coupled together. As noise increases ($\sigma = 2$ to $\sigma = 6$), the interaction between the bright and dark components becomes more pronounced. The bright peak broadens and loses height, while the dark trough becomes shallower and wider. The overall structure becomes less distinct, indicating a breakdown in the coupling between the bright and dark components. Straddled bright-dark solitons represent a hybrid soliton form that combines the properties of both bright and dark solitons. They maintain their structure under moderate noise but become increasingly unstable as noise intensity rises. The interaction between the bright and dark components becomes less coherent under high noise, leading to a loss of the soliton's hybrid nature.

Figures 31–36 explore the straddled singular-singular soliton $q(x, t)$ described by the complex-valued solution (42). These solitons feature two closely spaced singularities, each characterized by a sharp peak and steep gradient. The surface plots show that the soliton retains its dual singular structure over time, with both peaks maintaining their sharpness. With increasing noise ($\sigma = 2$ to $\sigma = 6$), the dual singular structure becomes increasingly disrupted. The peaks begin to flatten, and the steep gradients become less pronounced. The contour and 2D plots indicate that the soliton's singular nature is compromised, with the two singularities becoming less distinct and eventually merging into a broader, less defined structure. Straddled singular-singular solitons are characterized by the presence of two distinct singularities in close proximity. These solitons are stable in the absence of noise but are highly sensitive to noise, with the dual singular structure breaking down rapidly under increasing noise intensity. The soliton's ability to maintain distinct singularities diminishes as noise increases, leading to a loss of its characteristic structure. The analysis of various types of optical solitons under different conditions reveals the following key insights: Bright solitons are stable and robust under noise-free conditions but become increasingly unstable as noise intensity rises. The power nonlinearity parameter n plays a crucial role in determining the soliton's confinement and sensitivity to noise. Singular solitons exhibit strong localization and steep gradients, making them highly sensitive to noise. Even small amounts of noise can significantly disrupt their structure. Dark solitons maintain stability in the absence of noise but are less robust against noise compared to bright solitons.

The introduction of noise leads to a shallower and broader trough. Straddled bright-dark solitons combine the properties of bright and dark solitons. They are moderately stable under noise but lose their distinct structure as noise intensity increases. Straddled singular-singular solitons characterized

by dual singularities are highly sensitive to noise. The distinct singular structure breaks down rapidly under noise, leading to a loss of the soliton's characteristic features. Overall, the study highlights the critical role of noise and nonlinearity in determining the stability and behavior of optical solitons. While bright and dark solitons exhibit some resilience to noise, singular and hybrid solitons are more vulnerable, with their structure deteriorating rapidly under increasing noise intensity. The findings emphasize the need for careful consideration of environmental factors, such as noise and nonlinearity, in the practical application and manipulation of optical solitons.

Numerous experimental studies have confirmed the accuracy and physical relevance of soliton solutions in various nonlinear systems, particularly in nonlinear optics and fluid dynamics. Early pioneering works, such as Mollenauer et al. [26] and Hasegawa and Tappert [27], provided clear experimental evidence for soliton propagation in optical fibers, validating theoretical predictions in nonlinear optics. These studies demonstrated the fundamental properties of soliton behavior, such as pulse narrowing and stabilization in dispersive media. Similarly, Grimshaw [28] analyzed solitary waves in shallow water, highlighting their relevance in hydrodynamics and offering experimental insights that corroborate analytical soliton solutions in nonlinear evolution equations.

More recently, Herr et al. [29] and Kippenberg et al. [30] reported the generation and stabilization of temporal solitons in optical microresonators, representing a significant advancement in nonlinear optics. These studies not only confirmed the existence of solitons in new physical systems but also underscored their potential for practical applications, such as optical frequency comb generation. In parallel, Chabchoub et al. [31] observed soliton-like rogue waves in a water tank experiment, demonstrating the physical manifestation of nonlinear wave dynamics in fluid systems.

Although the current study has not directly verified the solutions of the Chen–Lee–Liu equation through experiments, the consistency between soliton solutions and experimental results in similar nonlinear systems provides strong evidence of their physical relevance. Therefore, the soliton solutions presented here can serve as reliable predictions for future experimental validation, further contributing to the understanding of nonlinear wave phenomena.

5. Conclusions

This article has successfully introduced a groundbreaking formulation of the CLL equation, which represents a significant leap forward in the field of nonlinear optics. By integrating multiplicative white noise within the Itô calculus framework, this study has expanded the theoretical landscape of the CLL equation, enabling researchers to analyze and predict complex optical phenomena under stochastic influences. This advancement not only broadens the mathematical understanding of the equation itself but also enhances its applicability in modeling real-world scenarios where noise and randomness play critical roles, such as in fiber optics and photonics.

The adoption of the improved extended modified tanh-function algorithm has proven instrumental in exploring the intricate soliton solutions of this stochastic system. This sophisticated method has enabled a comprehensive investigation, leading to the identification of a diverse spectrum of soliton types, including singular solitons, dark solitons, and bright solitons. These findings provide deep insights into the behavior and dynamics of solitons under the influence of stochastic perturbations. The detailed characterization of these solitons enhances our understanding of their stability, interaction properties, and potential for practical applications, such as in signal transmission and

energy propagation in nonlinear media.

The implications of these discoveries are far-reaching. By elucidating the intricate dynamics of solitons in the presence of stochasticity, this study paves the way for future research into their underlying mechanisms and properties. It highlights the importance of extending this work to more complex systems and different types of noise to uncover additional soliton behaviors and broaden the scope of their applications. Moreover, the results underscore the potential for leveraging these findings in designing advanced optical systems, such as noise-resilient communication networks and novel photonic devices.

As we look ahead, the foundational work established by this study opens up new avenues for interdisciplinary research, offering exciting opportunities to explore the role of solitons in a variety of scientific domains. The potential applications extend beyond nonlinear optics, with promising implications for fields such as quantum computing, biological systems, and even the study of complex networks. By addressing the interplay between nonlinearity, stochasticity, and soliton dynamics, this research represents a significant step forward in our ability to manipulate and understand complex physical systems. It serves as a catalyst for innovation, inspiring future investigations that could revolutionize our approach to solving challenges in science and engineering.

Author contributions

Ahmed M. Elsherbeny: Writing – original draft; Taher A. Nofal: Writing – original draft; Yakup Yıldırım: Writing – review & editing; Ahmed H. Arnous: Writing – review & editing. All authors have read and agreed to the published version of the manuscript.

Use of Generative-AI tools declaration

The authors declare that they have not used Artificial Intelligence tools in the creation of this article.

Acknowledgments

Funding

Conflict of interest

All authors declare no conflicts of interest in this paper.

References

1. A. Biswas, Topological 1-soliton solution of the nonlinear schrodinger's equation with Kerr law nonlinearity in 1+2 dimensions, *Commun. Nonlinear Sci.*, **14** (2009), 2845–2847. https://doi.org/10.1016/j.cnsns.2008.09.025

2. A. Biswas, H. Triki, 1-Soliton solution of the Klein–Gordon–Schrodinger's equation with power law nonlinearity, *Appl. Math. Comput.*, **217** (2010), 3869–3874. https://doi.org/10.1016/j.amc.2010.09.046

3. A. A. Al Qarni, M. A Banaja, H. O Bakodah, M. Mirzazadeh, A. Biswas, Optical solitons with coupled nonlinear Schrodinger's equation in birefringent nano-fibers by Adomian decomposition method, *J. Comput. Theor. Nanosci.*, **13** (2016), 5493–5498. https://doi.org/10.1166/jctn.2016.5444

4. N. A. Kudryashov, Conservation Laws of the Complex Ginzburg-Landau equation, *Phys. Lett. A*, **481** (2023), 128994. https://doi.org/10.1016/j.physleta.2023.128994

5. M. Y. Wang, Optical solitons with perturbed complex Ginzburg-Landau equation in Kerr and Cubic-Quintic-Septic nonlinearity, *Results Phys.*, **33** (2022), 105077. https://doi.org/10.1016/j.rinp.2021.105077

6. A. H. Arnous, A. R. Seadawy, R. T. Alqahtani, A. Biswas, Optical solitons with complex Ginzburg–Landau equation by modified simple equation method, *Optik*, **144** (2017), 475–480. https://doi.org/10.1016/j.ijleo.2017.07.013

7. N. A. Kudryashov, The Lakshmanan–Porsezian–Daniel Model with arbitrary refractive index and its solution, *Optik*, **241** (2021), 167043. https://doi.org/10.1016/j.ijleo.2021.167043

8. Y. Yıldırım, Optical soliton molecules of Lakshmanan–Porsezian–Daniel model in birefringent fibers by trial equation technique, *Optik*, **203** (2020), 162690. https://doi.org/10.1016/j.ijleo.2019.04.037

9. R. T. Alqahtani, M. M. Babatin, A. Biswas, Bright optical solitons for Lakshmanan-Porsezian-Daniel model by semi-inverse variational principle, *Optik*, **154** (2018), 109–114. https://doi.org/10.1016/j.ijleo.2017.09.112

10. H. H. Chen, Y. C. Lee, C. S. Liu, Integrability of nonlinear Hamiltonian systems by inverse scattering method, *Phys. Scr.*, **20** (1979), 490. https://doi.org/10.1088/0031-8949/20/3-4/026

11. Y. Yıldırım, Optical solitons to Chen–Lee–Liu model with trial equation approach, *Optik*, **183** (2019), 849–853. https://doi.org/10.1016/j.ijleo.2019.02.022

12. N. A. Kudryashov, Optical solitons of the Chen–Lee–Liu equation with arbitrary refractive index, *Optik*, **247** (2021), 167935. https://doi.org/10.1016/j.ijleo.2021.167935

13. A. Biswas, M. Ekici, A. Sonmezoglu, A. S. Alshomrani, Q. Zhou, S. P. Moshokoa, et al., Chirped optical solitons of Chen–Lee–Liu equation by extended trial equation scheme, *Optik*, **156** (2018), 999–1006. https://doi.org/10.1016/j.ijleo.2017.12.094

14. A. H. Arnous, M. Mirzazadeh, A. Akbulut, L. Akinyemi, Optical solutions and conservation laws of the Chen–Lee–Liu equation with Kudryashov's refractive index via two integrable techniques, *Wave. Random Complex*, 2022. https://doi.org/10.1080/17455030.2022.2045044

15. E. M. E. Zayed, A. H. Arnous, A. Secer, M. Ozisik, M. Bayram, N. A. Shah, et al., Highly dispersive optical solitons in fiber Bragg gratings for stochastic Lakshmanan–Porsezian–Daniel equation with spatio-temporal dispersion and multiplicative white noise, *Results Phys.*, **55** (2023), 107177. https://doi.org/10.1016/j.rinp.2023.107177

16. E. M. E. Zayed, A. H. Arnous, A. Biswas, Y. Yıldırım, A. Asiri, Optical solitons for the concatenation model with multiplicative white noisee, *J. Opt.*, **53** (2024), 3098–3107. https://doi.org/10.1007/s12596-023-01381-w

17. A. Secer, Stochastic optical solitons with multiplicative white noise via Itô calculus, *Optik*, **268** (2022), 169831. https://doi.org/10.1016/j.ijleo.2022.169831

18. Z. Li, C. Peng, Dynamics and embedded solitons of stochastic quadratic and cubic nonlinear susceptibilities with multiplicative white noise in the Itô sense, *Mathematics*, **11** (2023), 3185. https://doi.org/10.3390/math11143185

19. H. Cakicioglu, M. Ozisik, A. Secer, M. Bayram, Stochastic dispersive Schrödinger–Hirota equation having parabolic law nonlinearity with multiplicative white noise via Ito calculus, *Optik*, **279** (2023), 170776. https://doi.org/10.1016/j.ijleo.2023.170776

20. K. Zhang, J. Cao, J. Lvu, Dynamic behavior and modulation instability for a generalized nonlinear Schrödinger equation with nonlocal nonlinearity, *Phys. Scr.*, **100** (2025), 015262. https://doi.org/10.1088/1402-4896/ad9cfa

21. S. Zhao, Z. Li, The analysis of traveling wave solutions and dynamical behavior for the stochastic coupled Maccari's system via Brownian motion, *Ain Shams Eng. J.*, **15** (2024), 103037. https://doi.org/10.1016/j.asej.2024.103037

22. W. W. Mohammed, S. Albosaily, N. Iqbal, M. El-Morshedy, The effect of multiplicative noise on the exact solutions of the stochastic Burgers' equation, *Wave. Random Complex*, **34** (2024), 274–286. https://doi.org/10.1080/17455030.2021.1905914

23. W. W. Mohammed, M. El-Morshedy, The influence of multiplicative noise on the stochastic exact solutions of the Nizhnik–Novikov–Veselov system, *Math. Comput. Simulat.*, **190** (2021), 192–202. https://doi.org/10.1016/j.matcom.2021.05.022

24. K. Itô, Stochastic integral, *Proc. Imp. Acad.*, **20** (1944), 519–524. https://doi.org/10.3792/pia/1195572786

25. Z. Yang, B. Y. C. Hon, An improved modified extended Tanh-function method, *Zeitschrift für Naturforschung A*, **61** (2006), 103–115. https://doi.org/10.1515/zna-2006-3-401

26. L. F. Mollenauer, R. H. Stolen, J. P. Gordon, Experimental observation of picosecond pulse narrowing and solitons in optical fibers, *Phys. Rev. Lett.*, **45** (1980), 1095–1098. https://doi.org/10.1103/PhysRevLett.45.1095

27. A. Hasegawa, F. Tappert, Transmission of stationary nonlinear optical pulses in dispersive dielectric fibers. I. Anomalous dispersion, *Appl. Phys. Lett.*, **23** (1973), 142–144. https://doi.org/10.1063/1.1654836

28. R. Grimshaw, The solitary wave in water of finite depth, *J. Fluid Mech.*, **42** (1970), 639–656. https://doi.org/10.1017/S0022112070001520

29. T. Herr, V. Brasch, J. D. Jost, C. Y. Wang, N. M. Kondratiev, M. L. Gorodetsky, et al., Temporal solitons in optical microresonators, *Nature Photon.*, **8** (2014), 145–152. https://doi.org/10.1038/nphoton.2013.343

30. T. J. Kippenberg, R. Holzwarth, S. A. Diddams, Microresonator-based optical frequency combs, *Science*, **332** (2011), 555–559. https://doi.org/10.1126/science.1193968

31. F. Chabchoub, N. P. Hoffmann, N. Akhmediev, Rogue wave observation in a water wave tank, *Phys. Rev. Lett.*, **106** (2011), 204502. https://doi.org/10.1103/PhysRevLett.106.204502

Appendix

(a) Surface plot   **(b)** Contour plot   **(c)** 2D plot

(d) Surface plot   **(e)** Contour plot   **(f)** 2D plot

(g) Surface plot   **(h)** Contour plot   **(i)** 2D plot
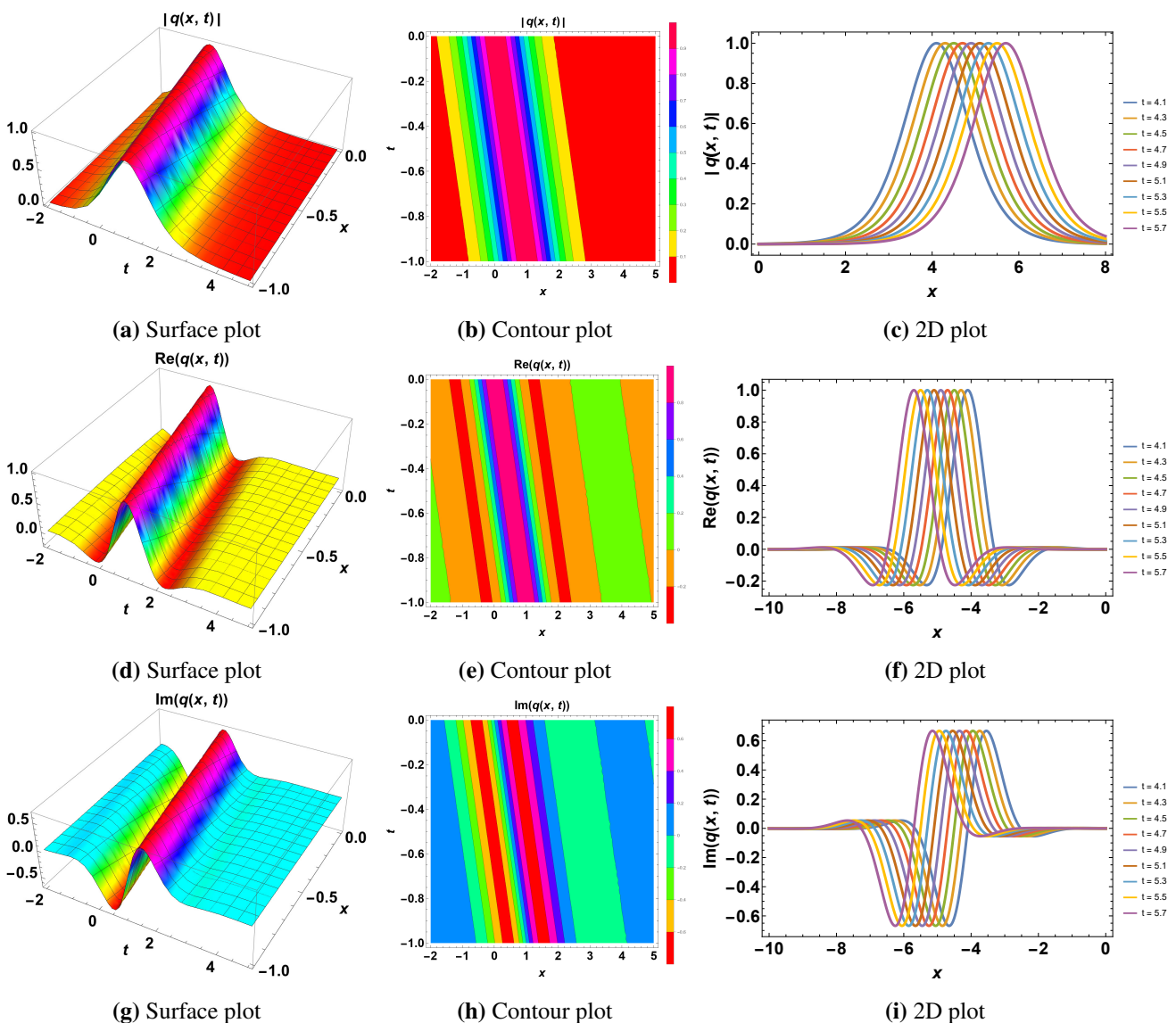
Figure 1. Profile of a bright soliton given $\sigma = 0$.
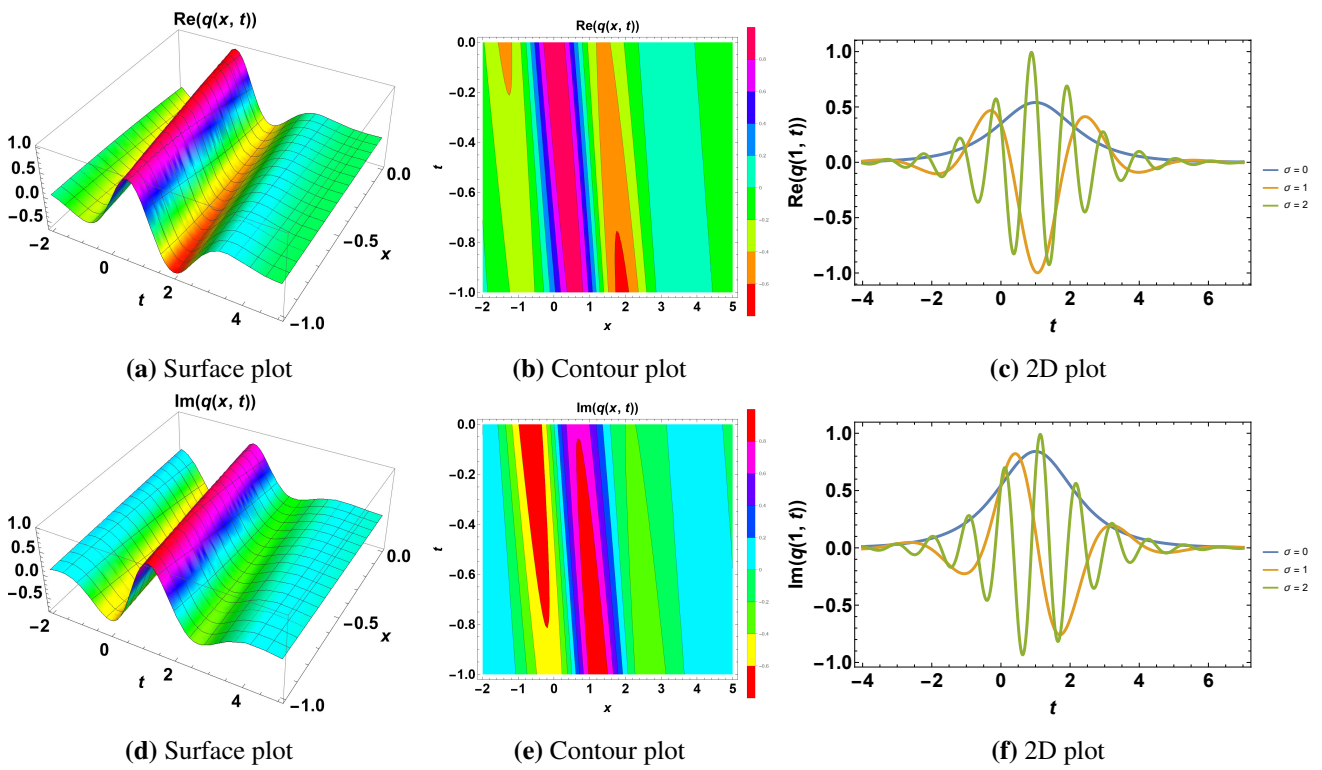
Figure 2. Profile of a bright soliton given $\sigma = 2$.
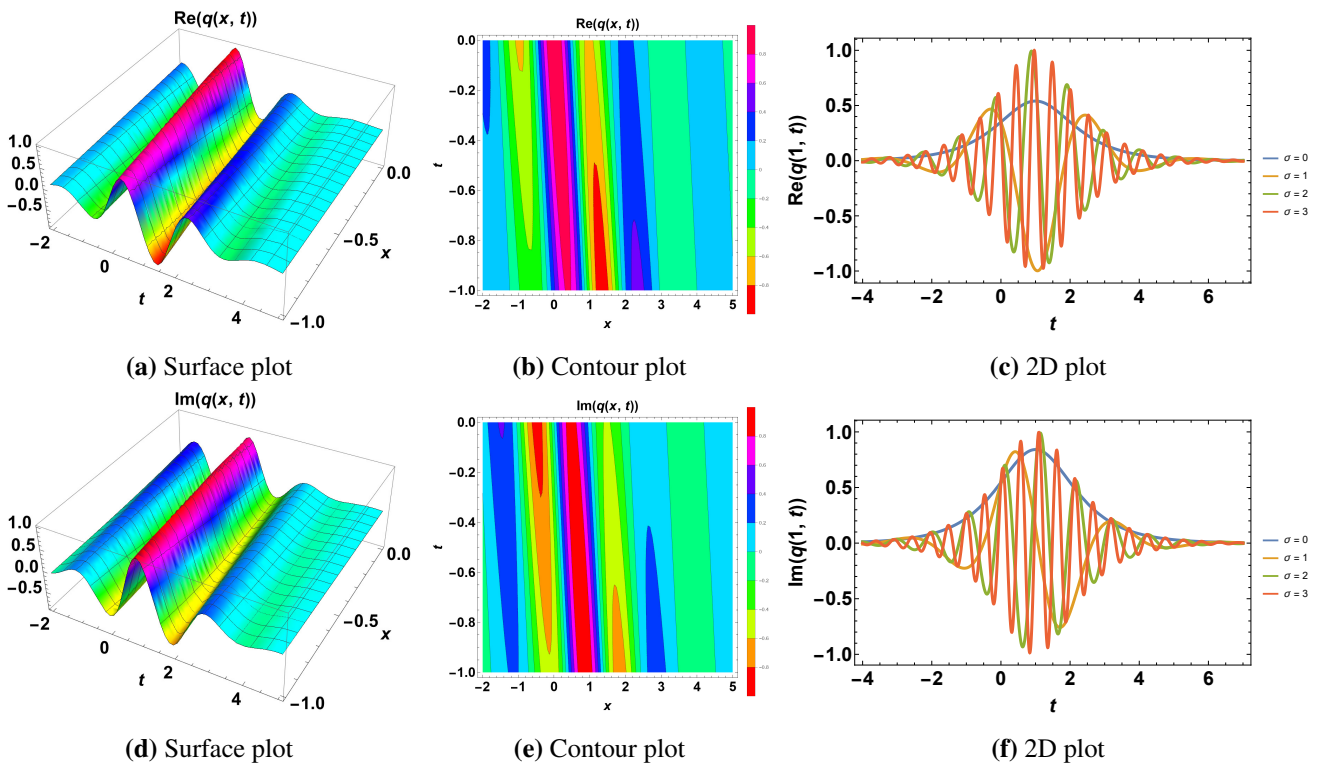
Figure 3. Profile of a bright soliton given $\sigma = 3$.
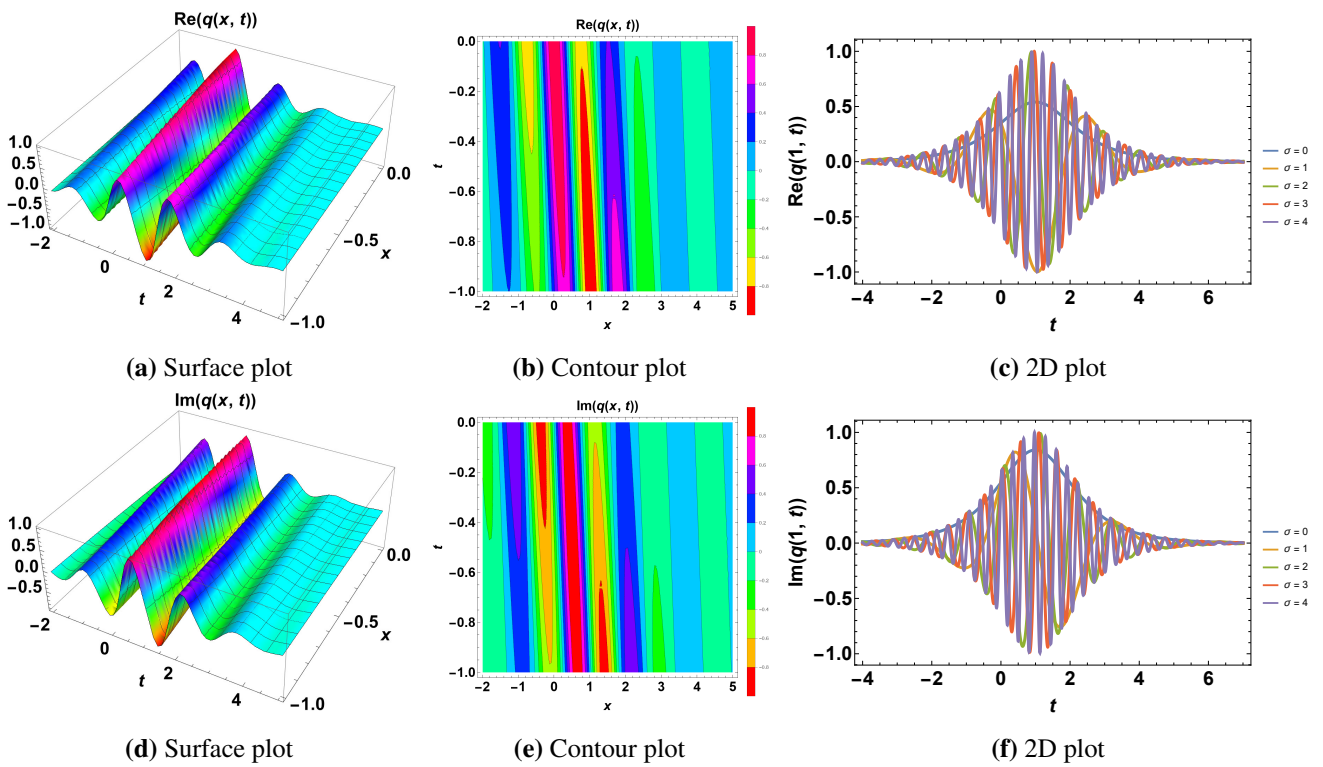
Figure 4. Profile of a bright soliton given $\sigma = 4$.
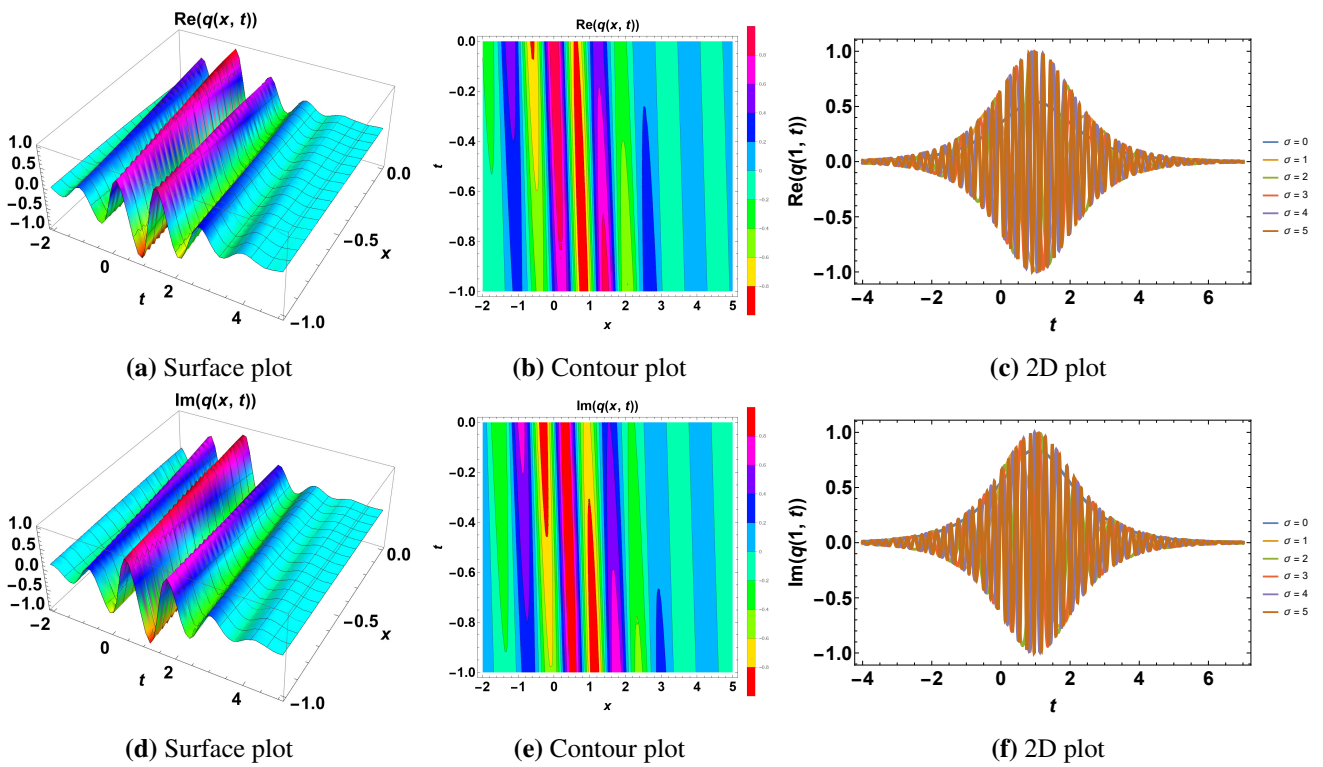
Figure 5. Profile of a bright soliton given $\sigma = 5$.
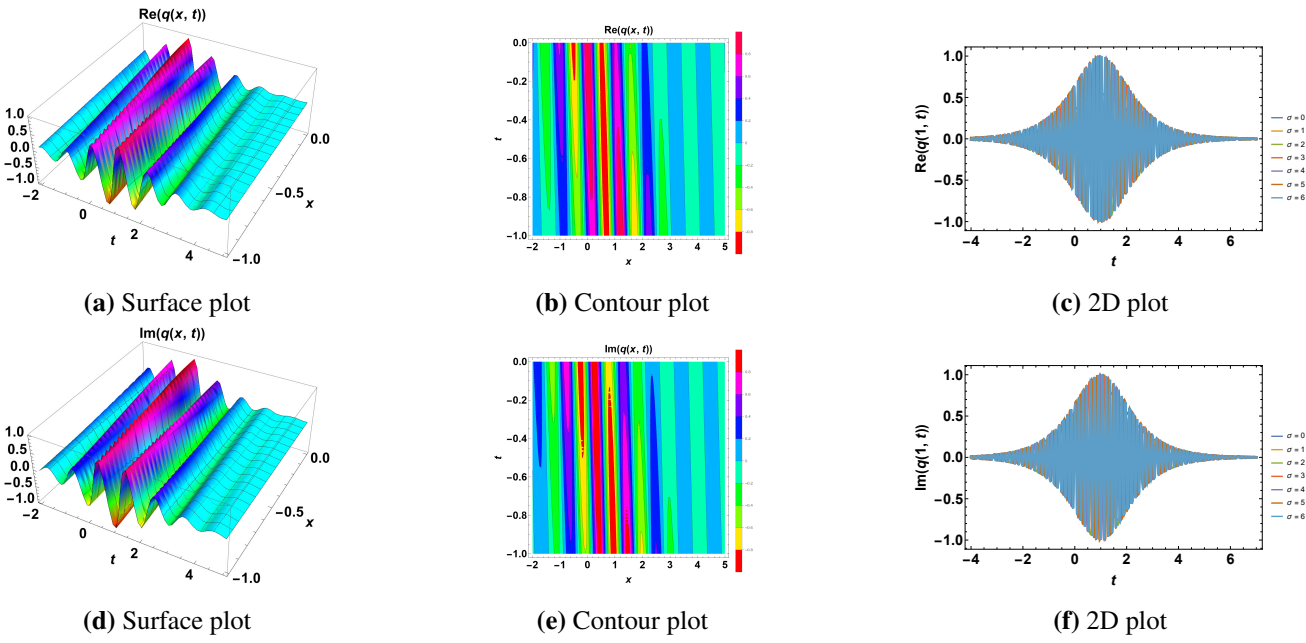
Figure 6. Profile of a bright soliton given $\sigma = 6$.
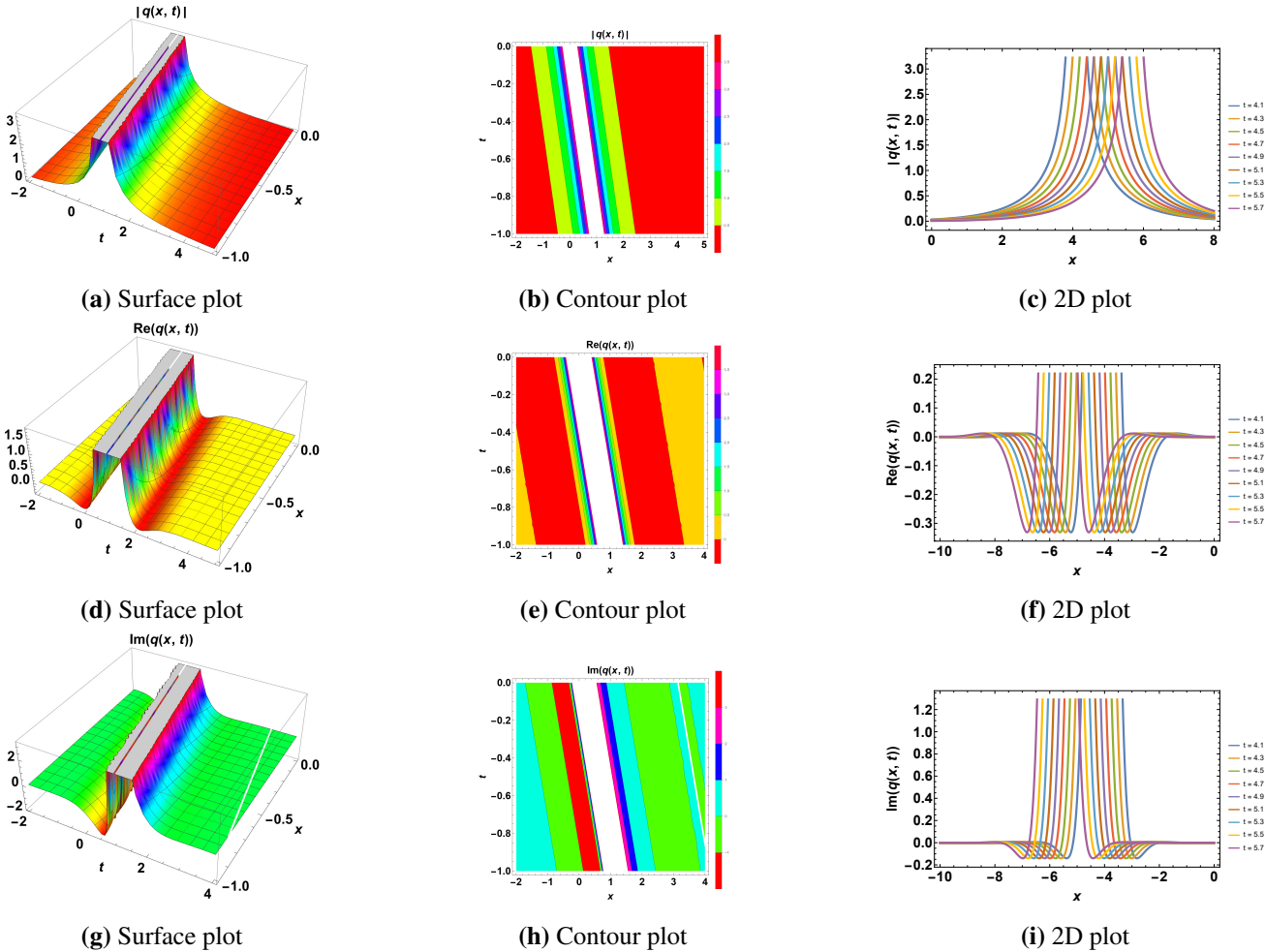
Figure 7. Profile of a singular soliton given $\sigma = 0$.
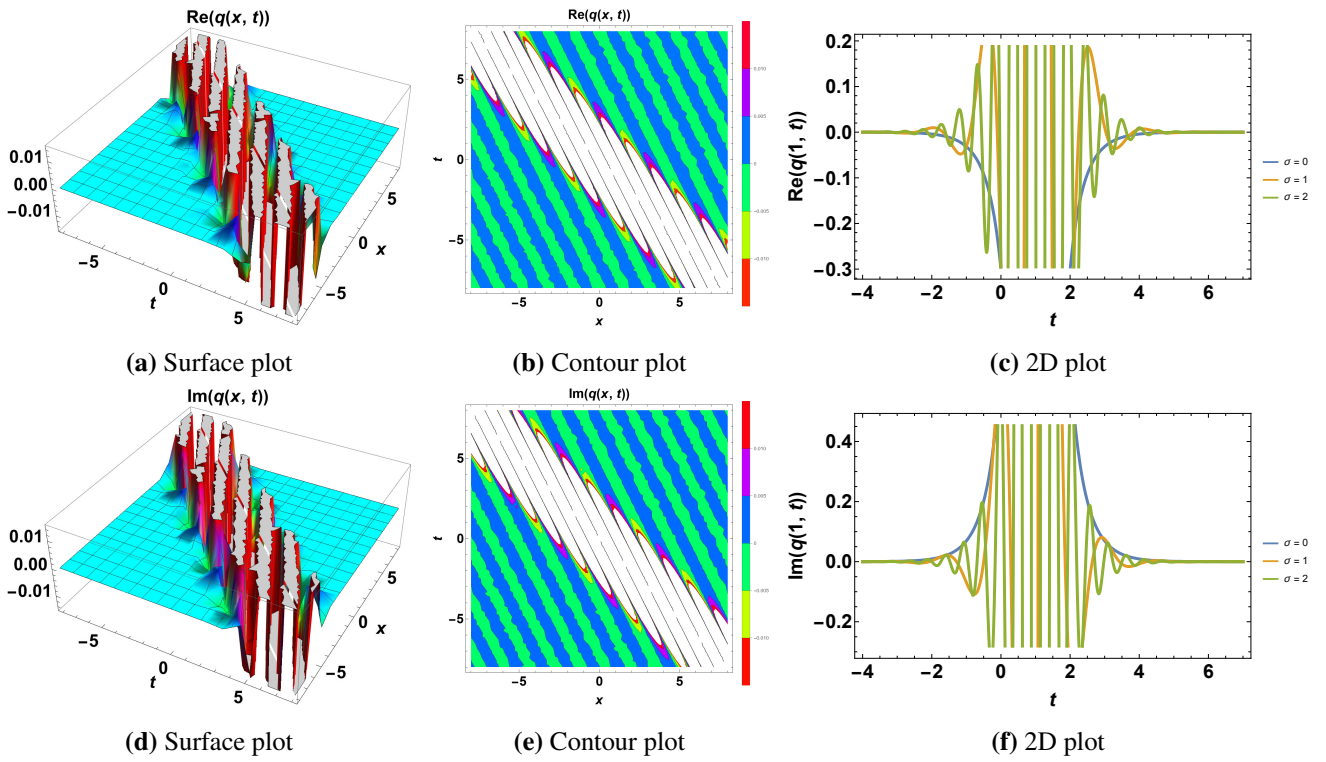
Figure 8. Profile of a singular soliton given $\sigma = 2$.
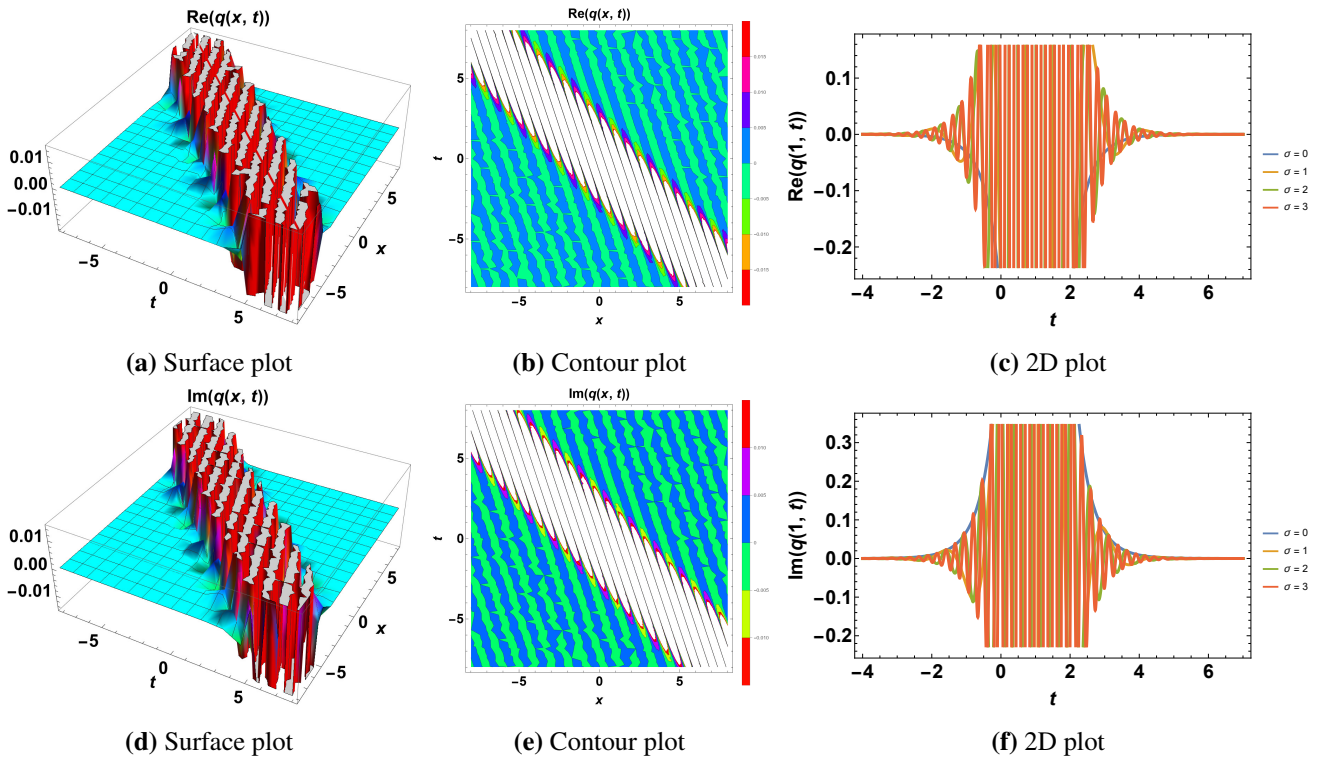
Figure 9. Profile of a singular soliton given $\sigma = 3$.
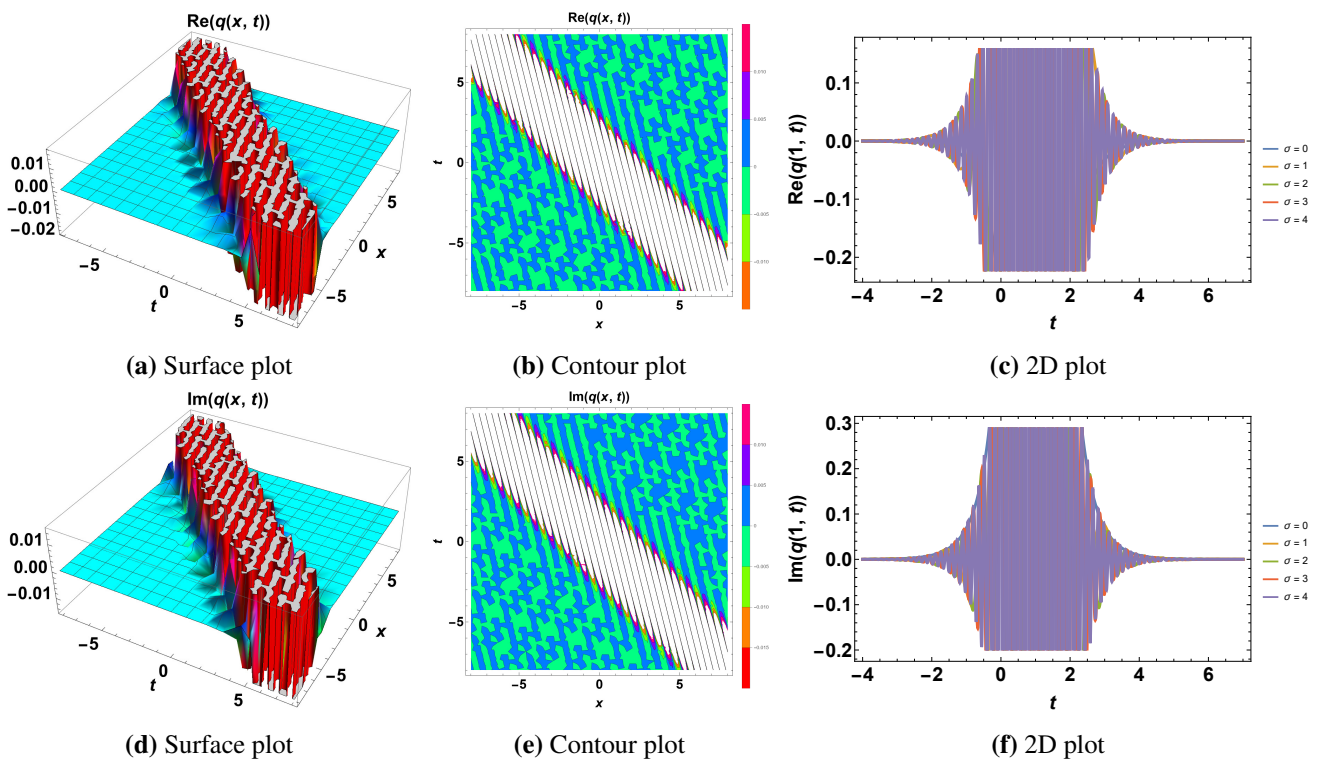
Figure 10. Profile of a singular soliton given $\sigma = 4$.
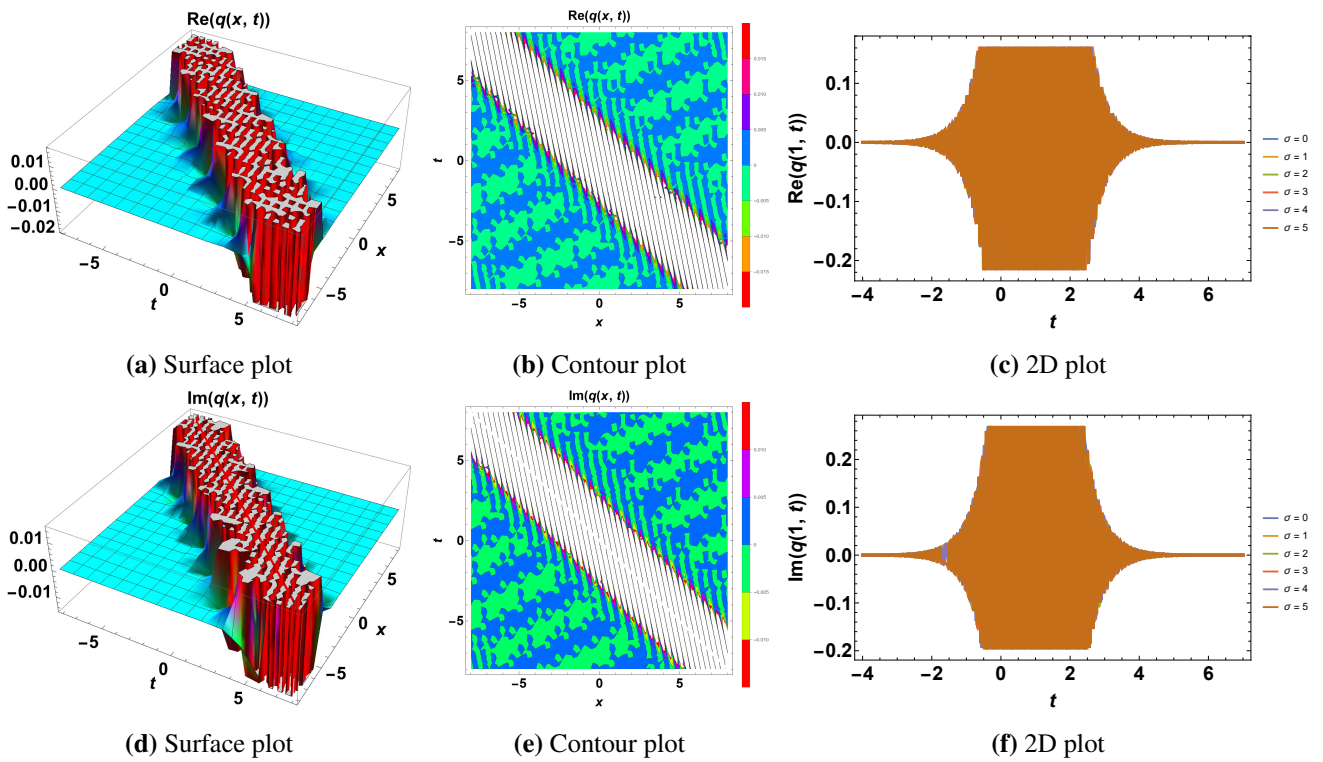
Figure 11. Profile of a singular soliton given $\sigma = 5$.
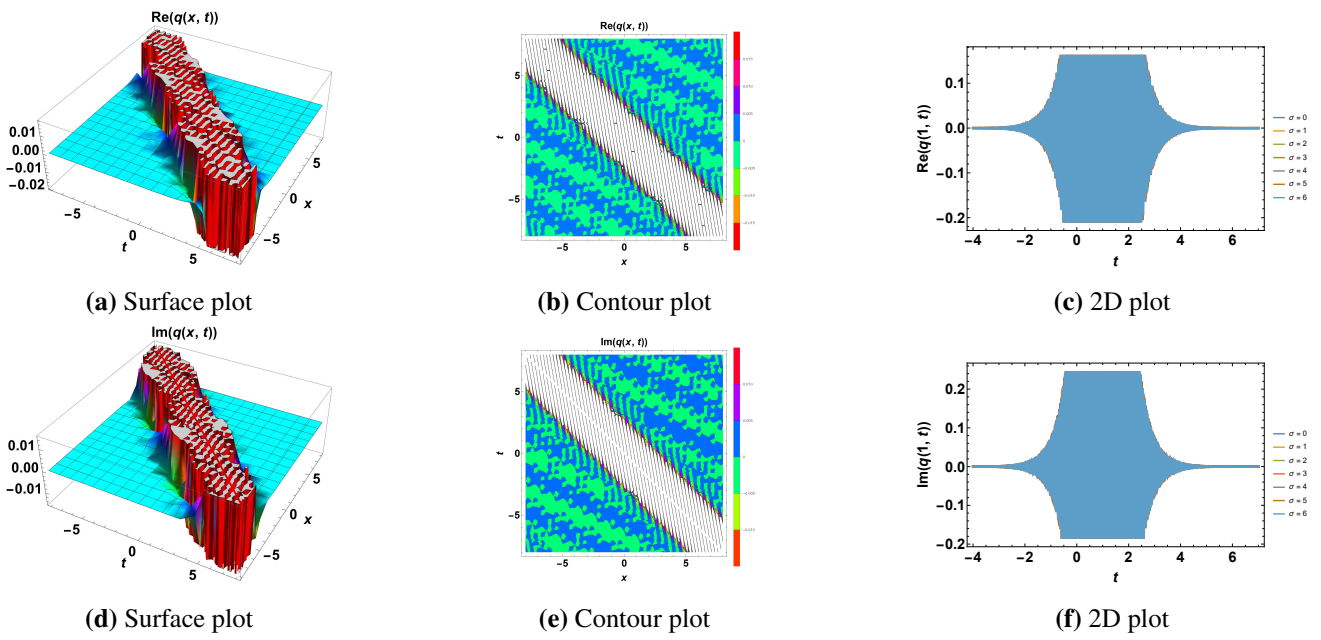
Figure 12. Profile of a singular soliton given $\sigma = 6$.
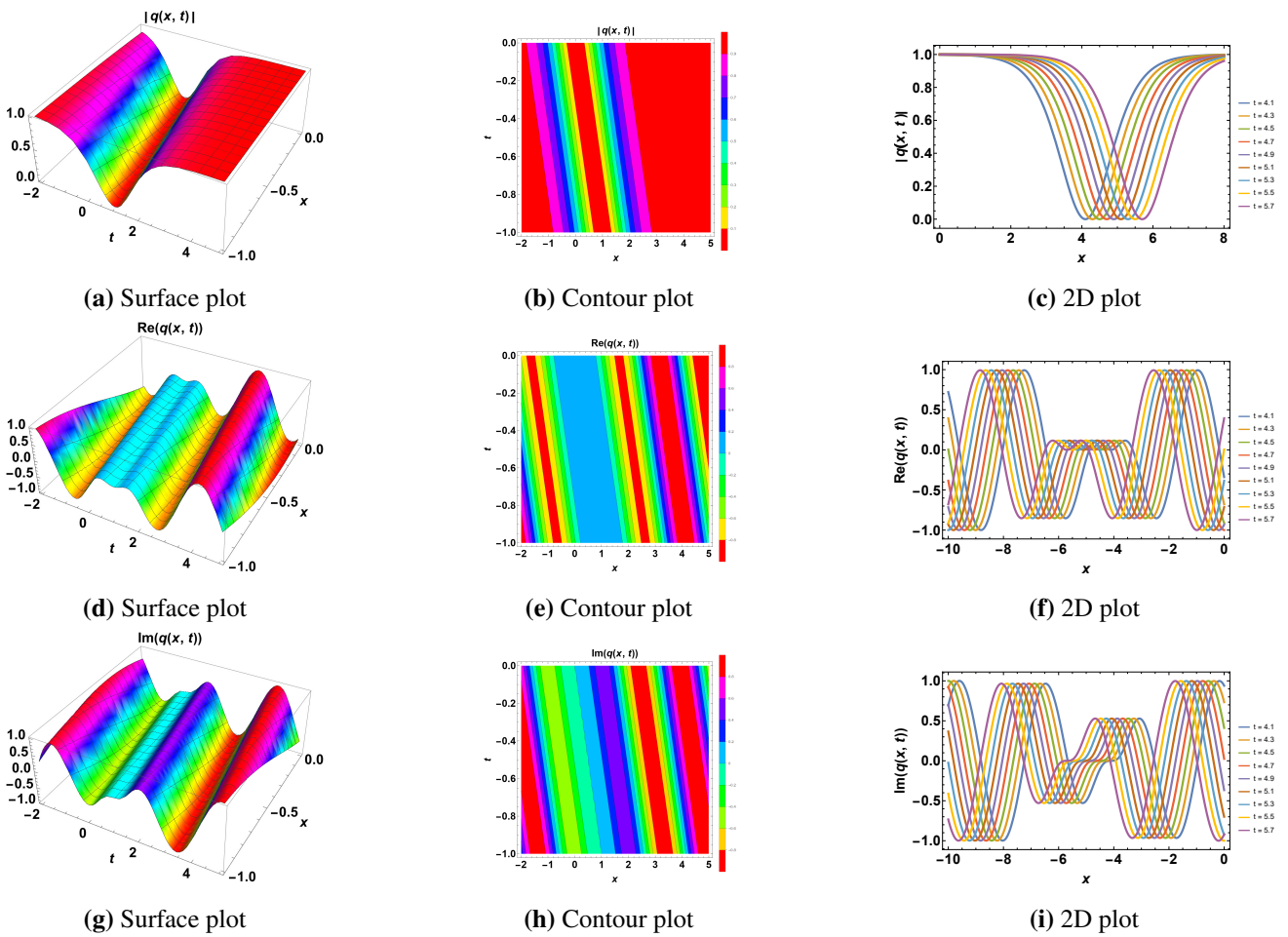
Figure 13. Profile of a dark soliton given $\sigma = 0$.
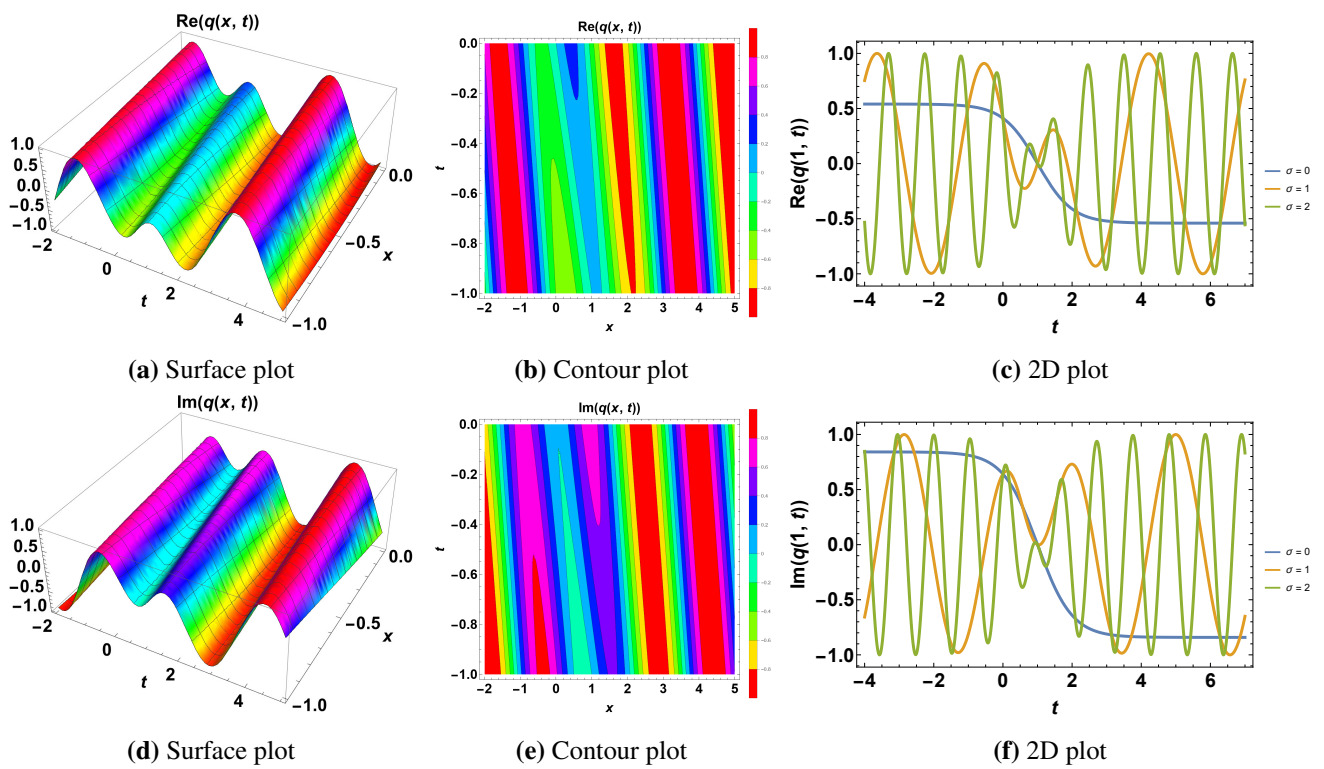
Figure 14. Profile of a dark soliton given $\sigma = 2$.
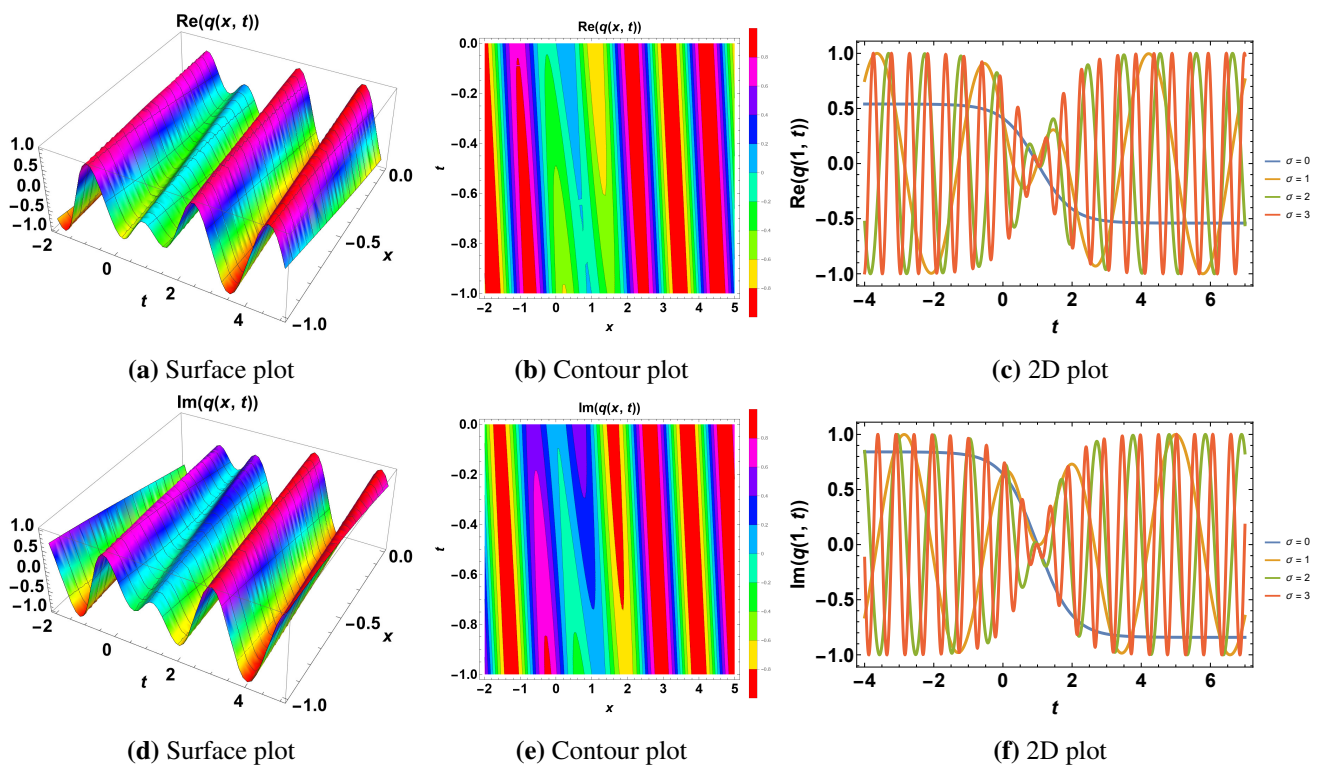
Figure 15. Profile of a dark soliton given $\sigma = 3$.

(a) Surface plot

(b) Contour plot

(c) 2D plot

(d) Surface plot

(e) Contour plot

(f) 2D plot
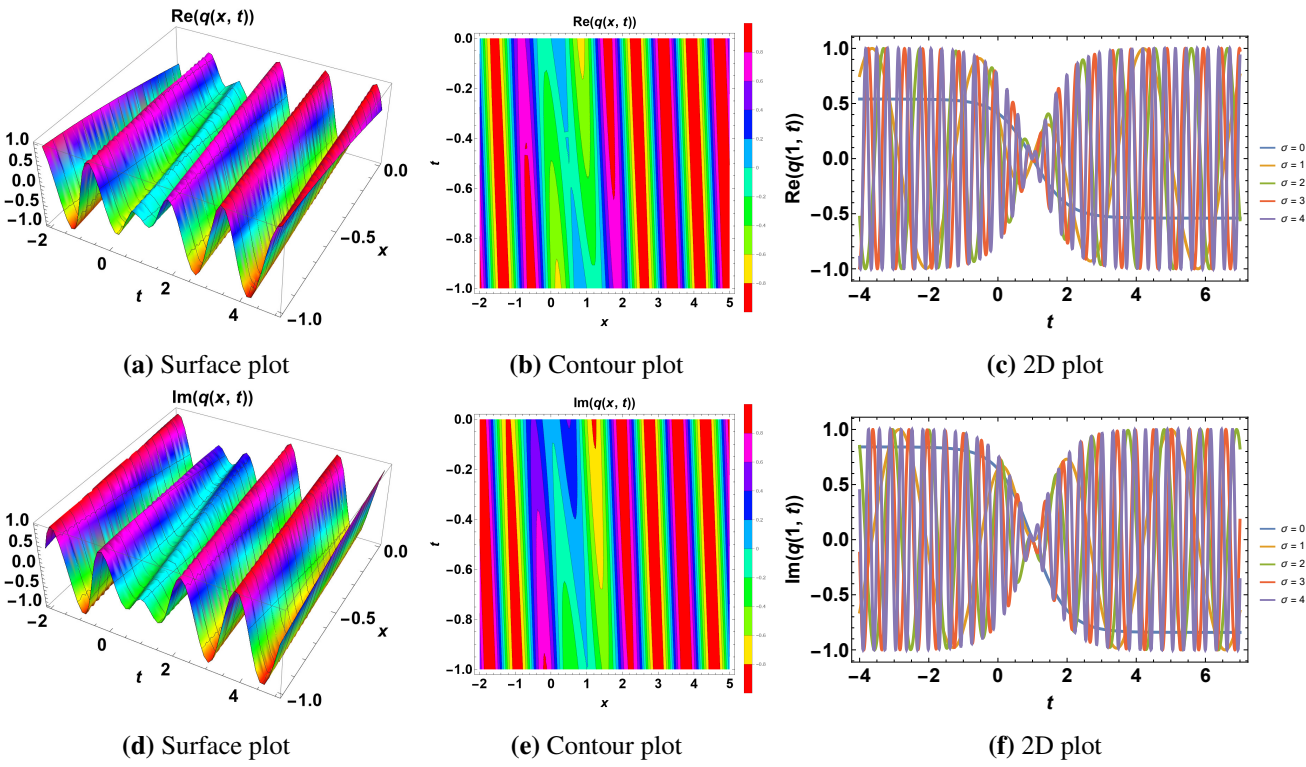
Figure 16. Profile of a dark soliton given $\sigma = 4$.

(a) Surface plot

(b) Contour plot

(c) 2D plot

(d) Surface plot

(e) Contour plot

(f) 2D plot
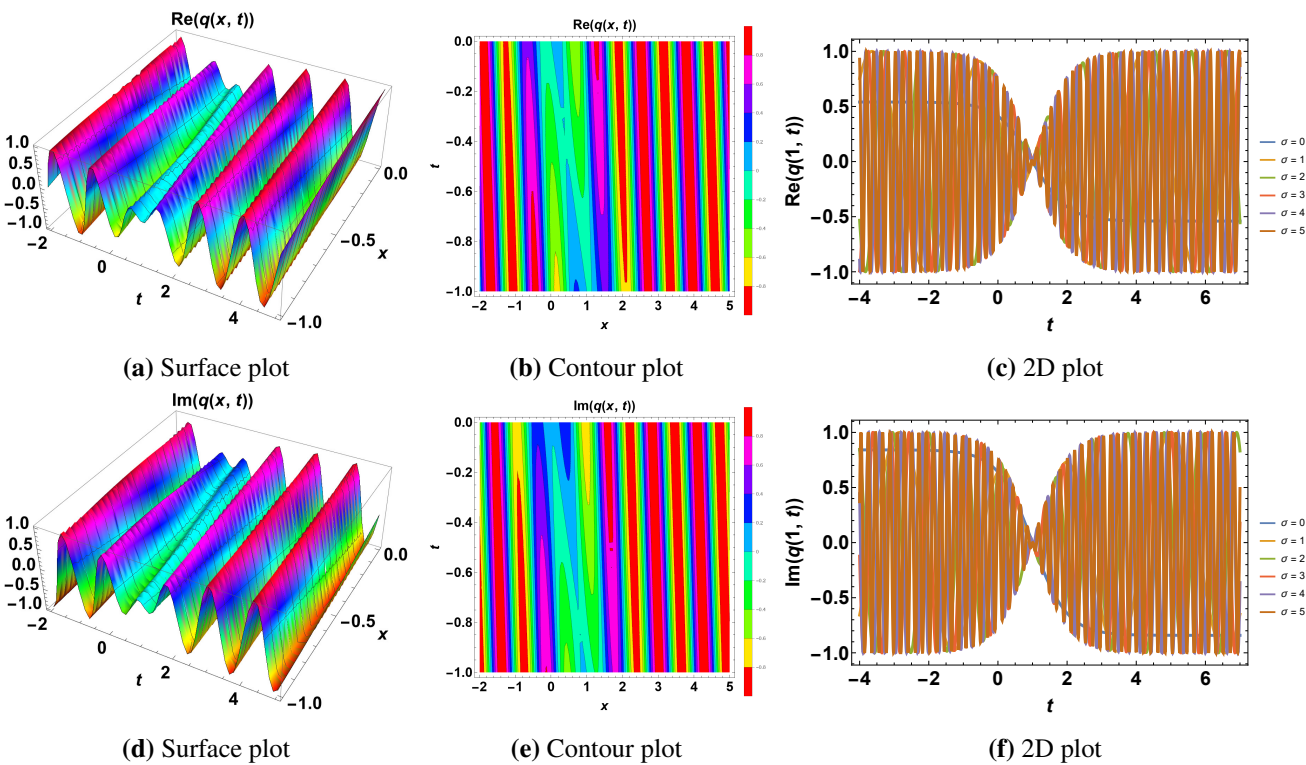
Figure 17. Profile of a dark soliton given $\sigma = 5$.

(a) Surface plot **(b)** Contour plot **(c)** 2D plot

(d) Surface plot **(e)** Contour plot **(f)** 2D plot
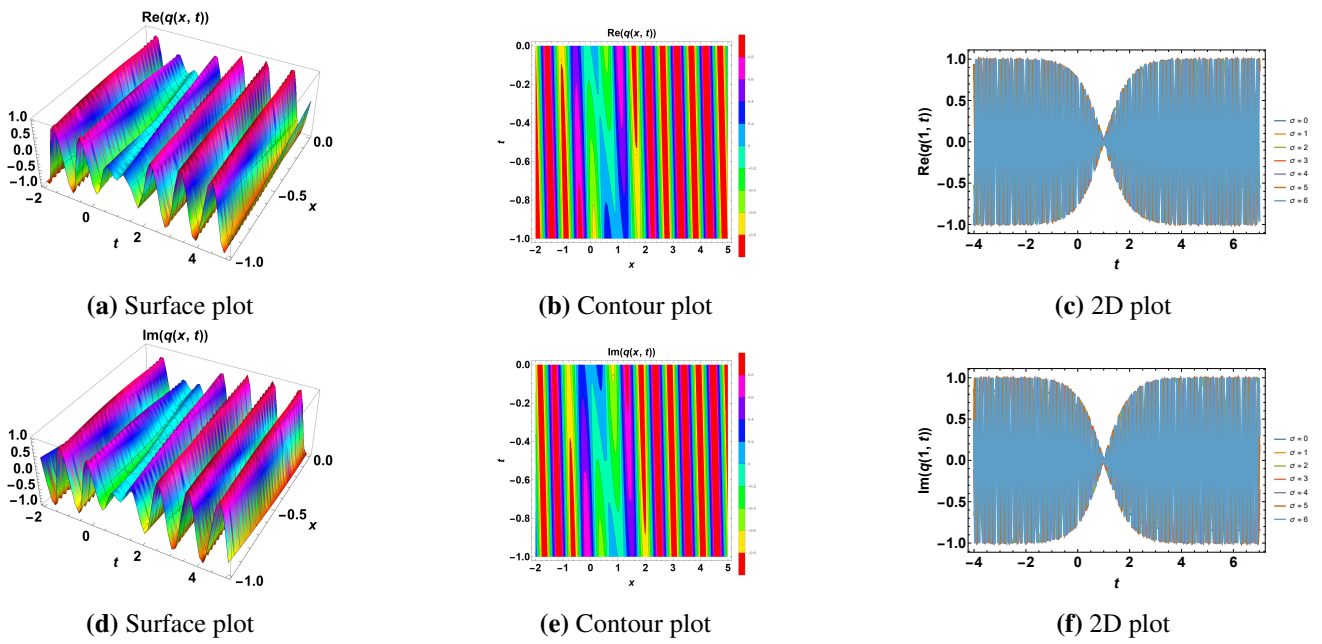
Figure 18. Profile of a dark soliton given $\sigma = 6$.

(a) Surface plot **(b)** Contour plot **(c)** 2D plot

(d) Surface plot **(e)** Contour plot **(f)** 2D plot

(g) Surface plot **(h)** Contour plot **(i)** 2D plot
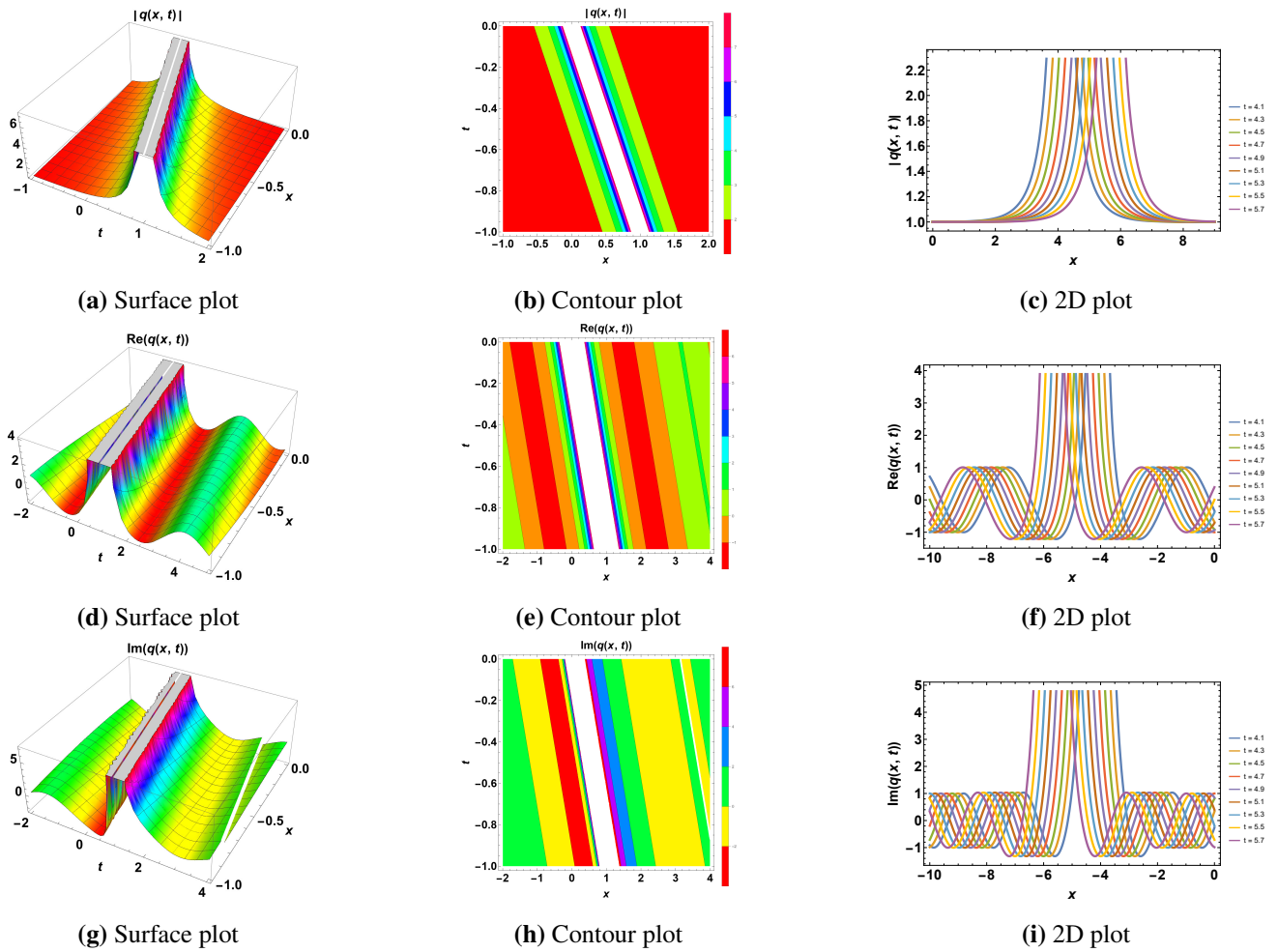
Figure 19. Profile of a singular soliton given $\sigma = 0$.
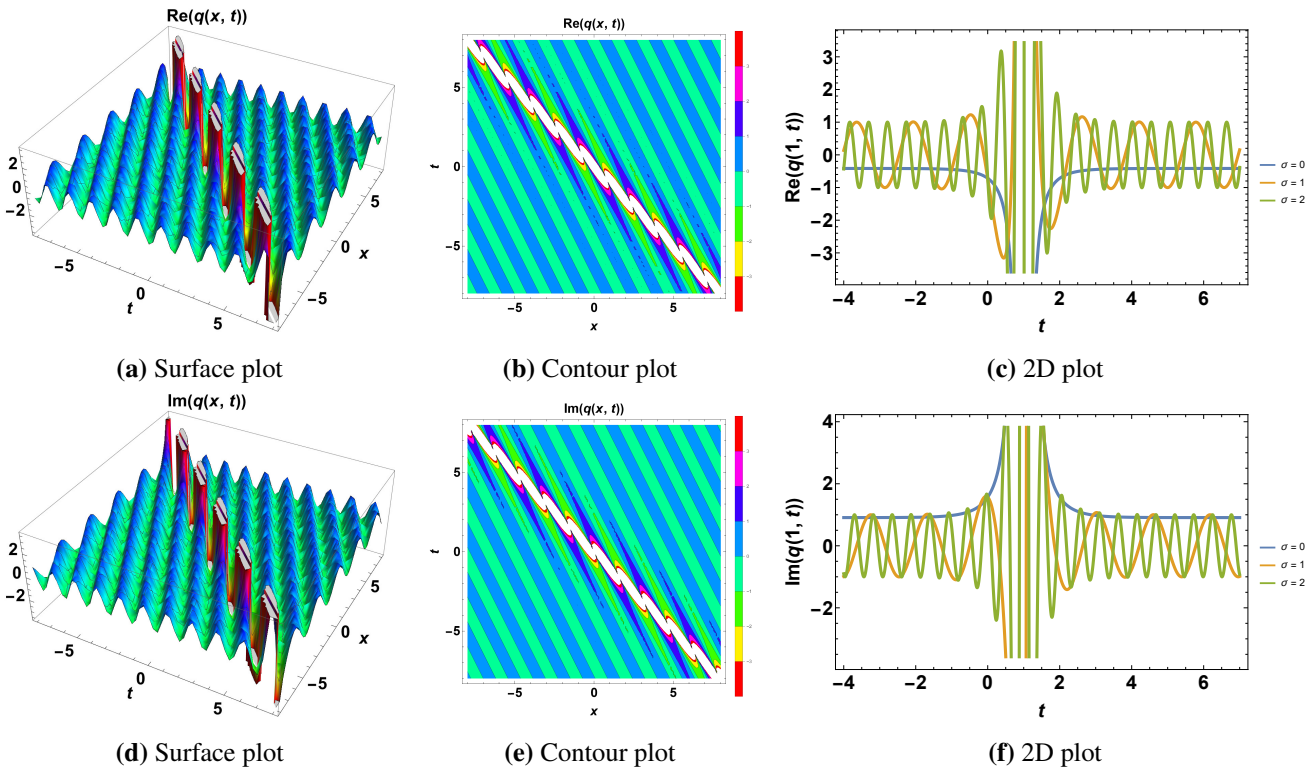
Figure 20. Profile of a singular soliton given $\sigma = 2$.
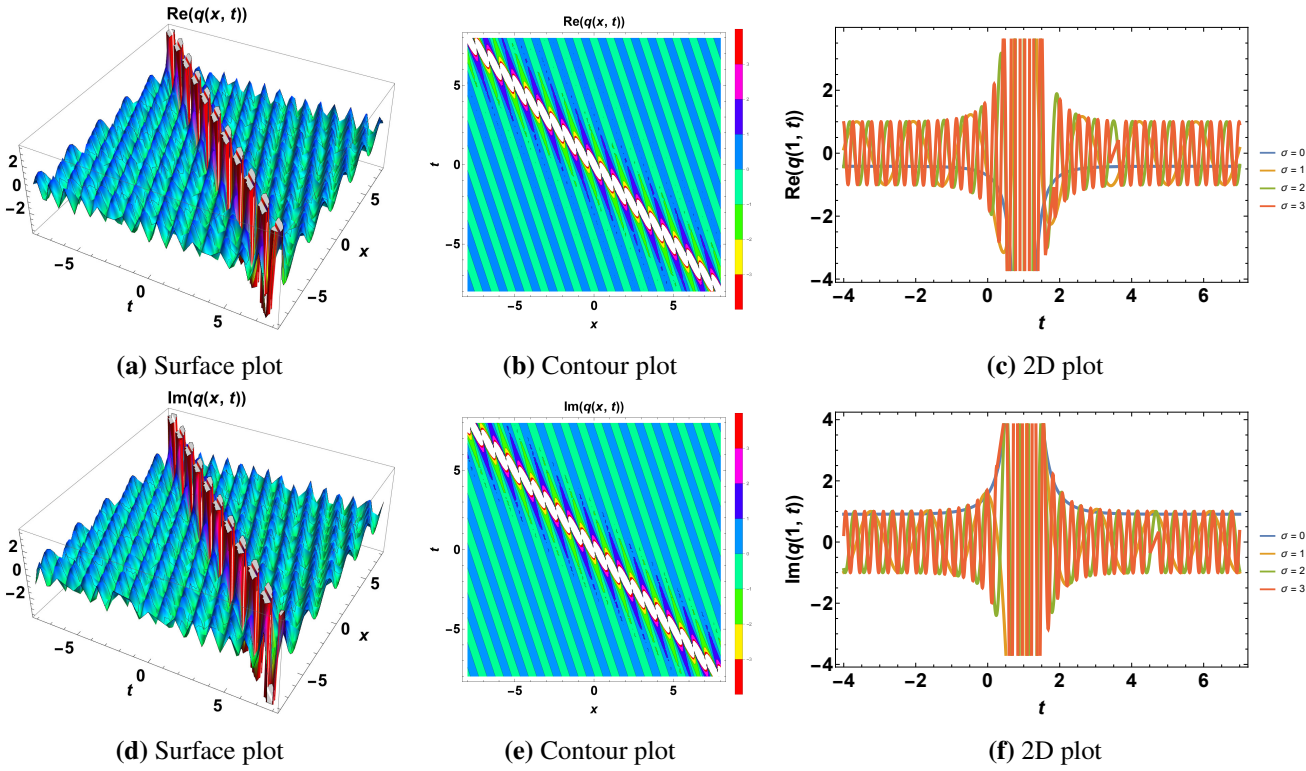
Figure 21. Profile of a singular soliton given $\sigma = 3$.
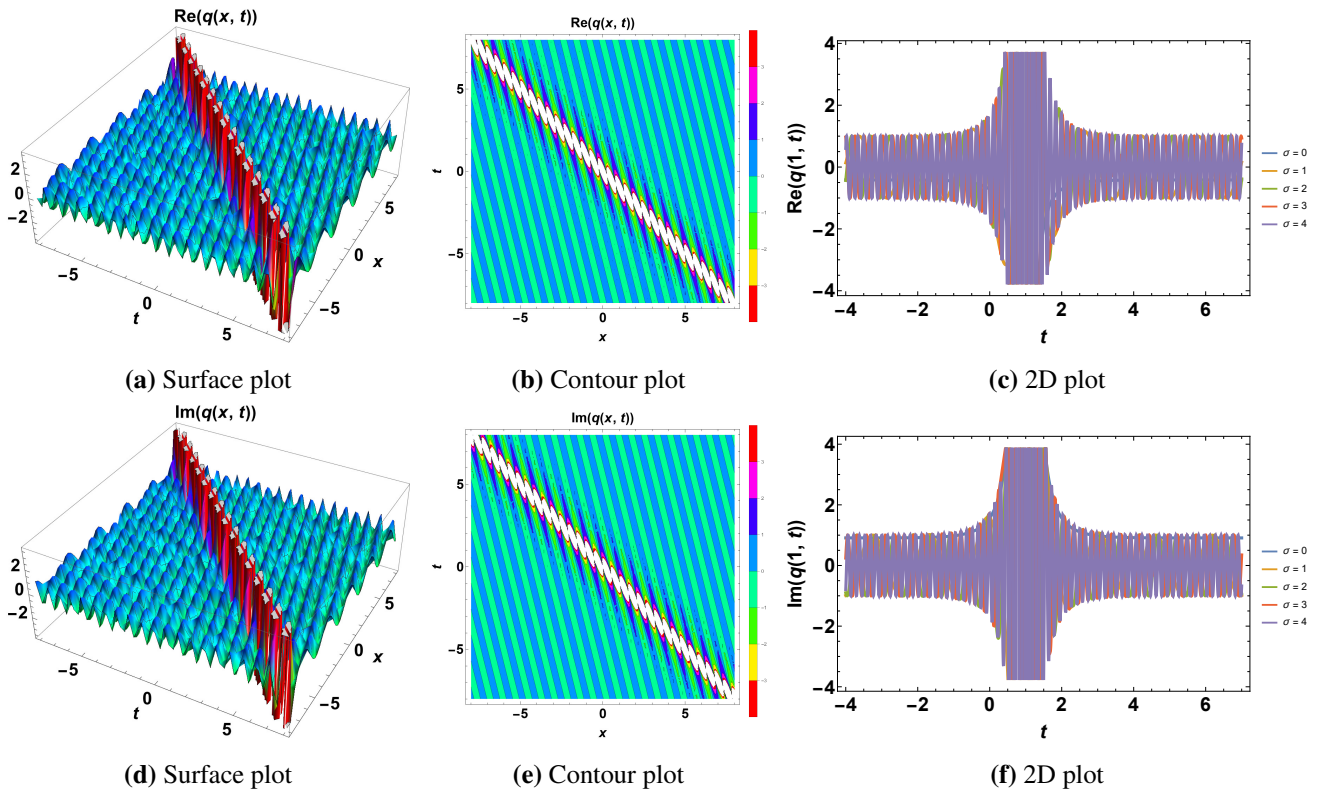
Figure 22. Profile of a singular soliton given $\sigma = 4$.
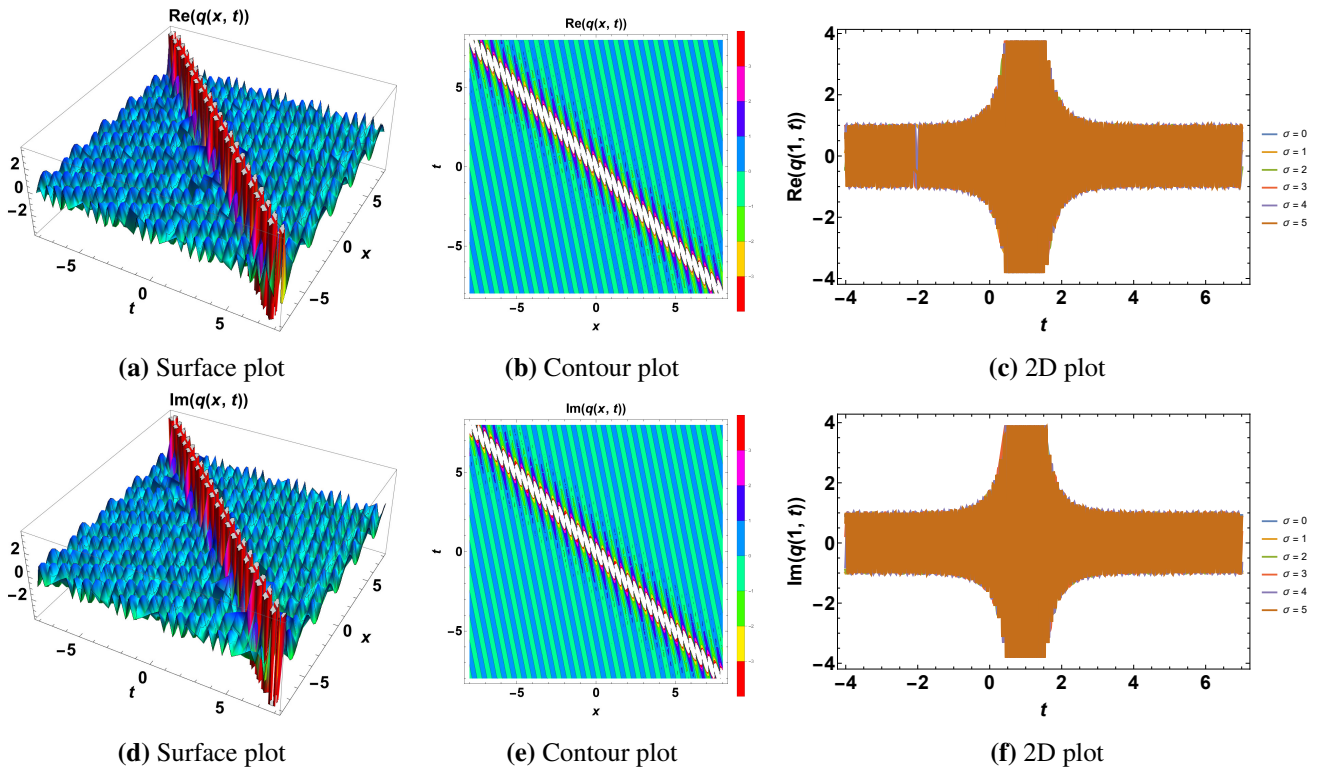
Figure 23. Profile of a singular soliton given $\sigma = 5$.

(a) Surface plot   **(b)** Contour plot   **(c)** 2D plot

(d) Surface plot   **(e)** Contour plot   **(f)** 2D plot
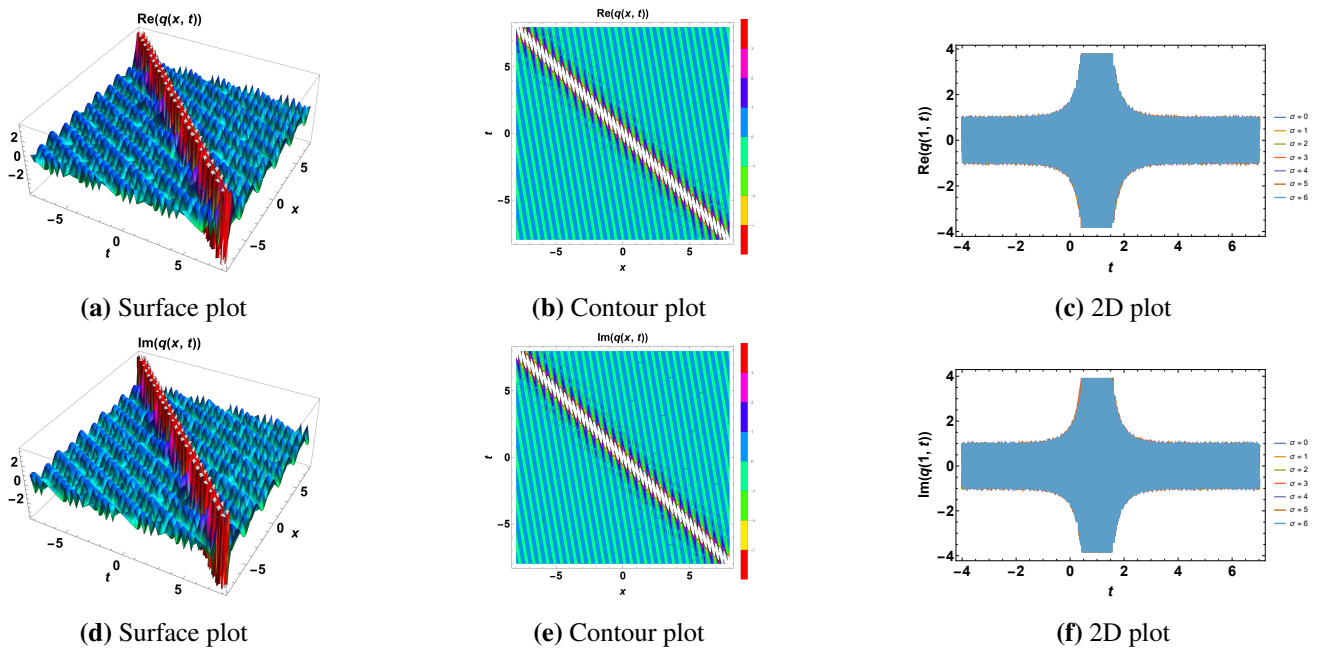
Figure 24. Profile of a singular soliton given $\sigma = 6$.

(a) Surface plot   **(b)** Contour plot   **(c)** 2D plot

(d) Surface plot   **(e)** Contour plot   **(f)** 2D plot

(g) Surface plot   **(h)** Contour plot   **(i)** 2D plot
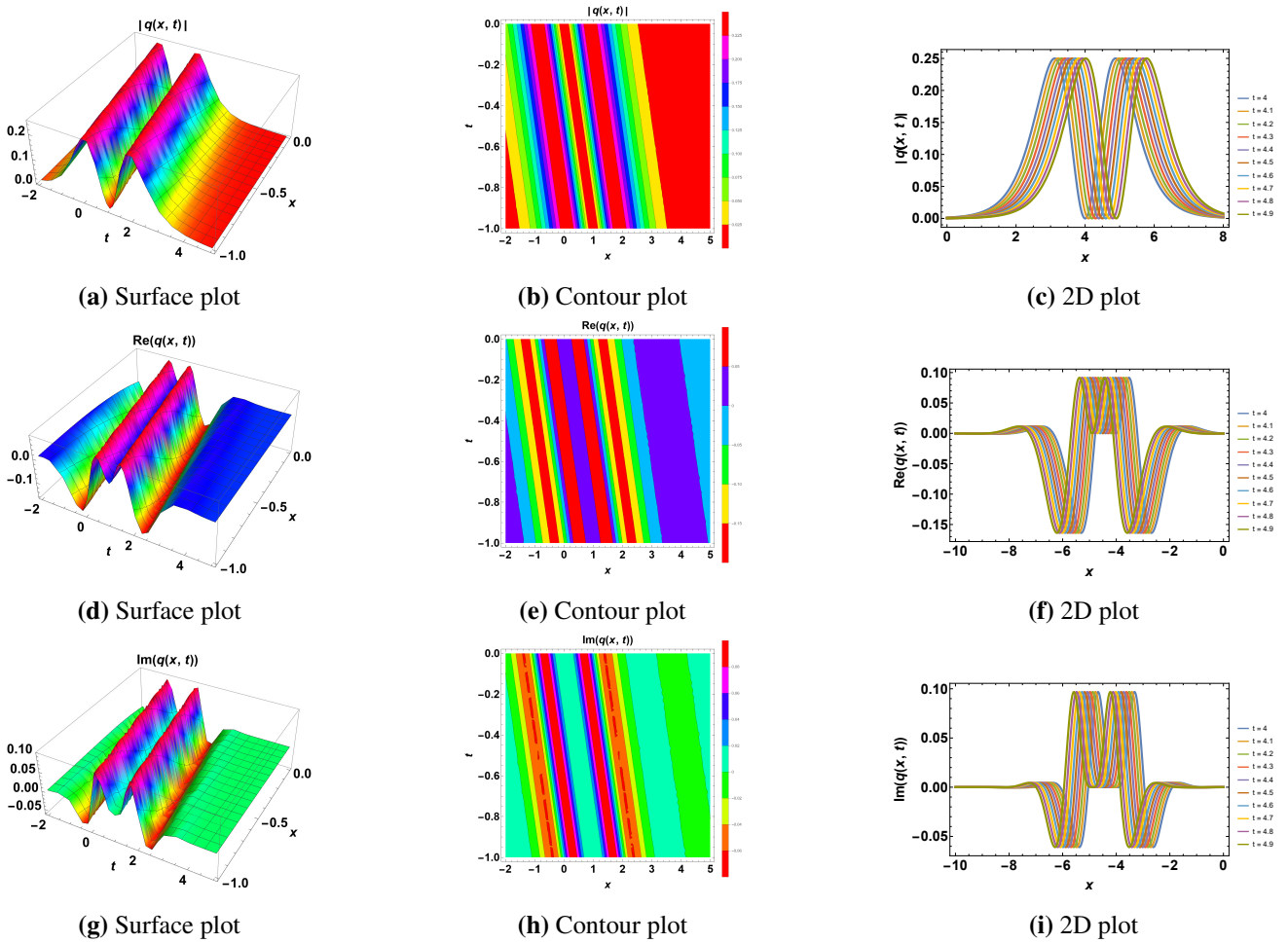
Figure 25. Profile of a bright-dark soliton given $\sigma = 0$.
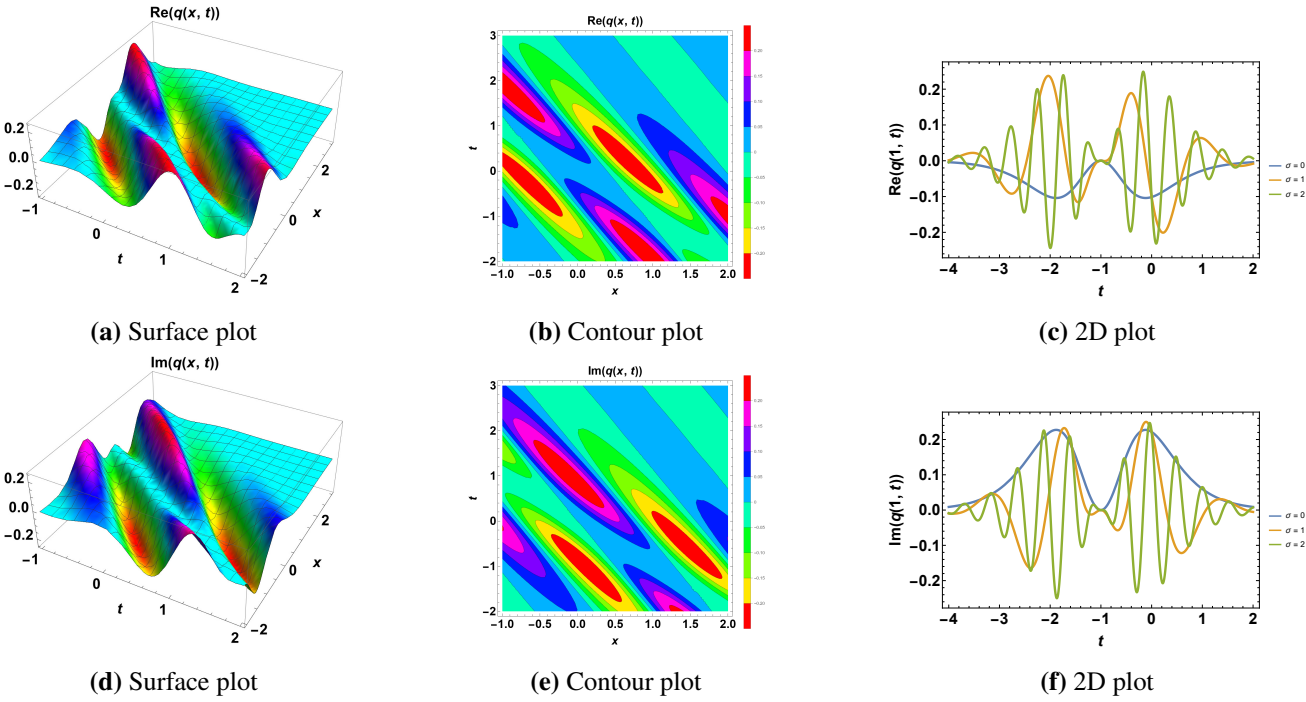
Figure 26. Profile of a bright-dark soliton given $\sigma = 2$.
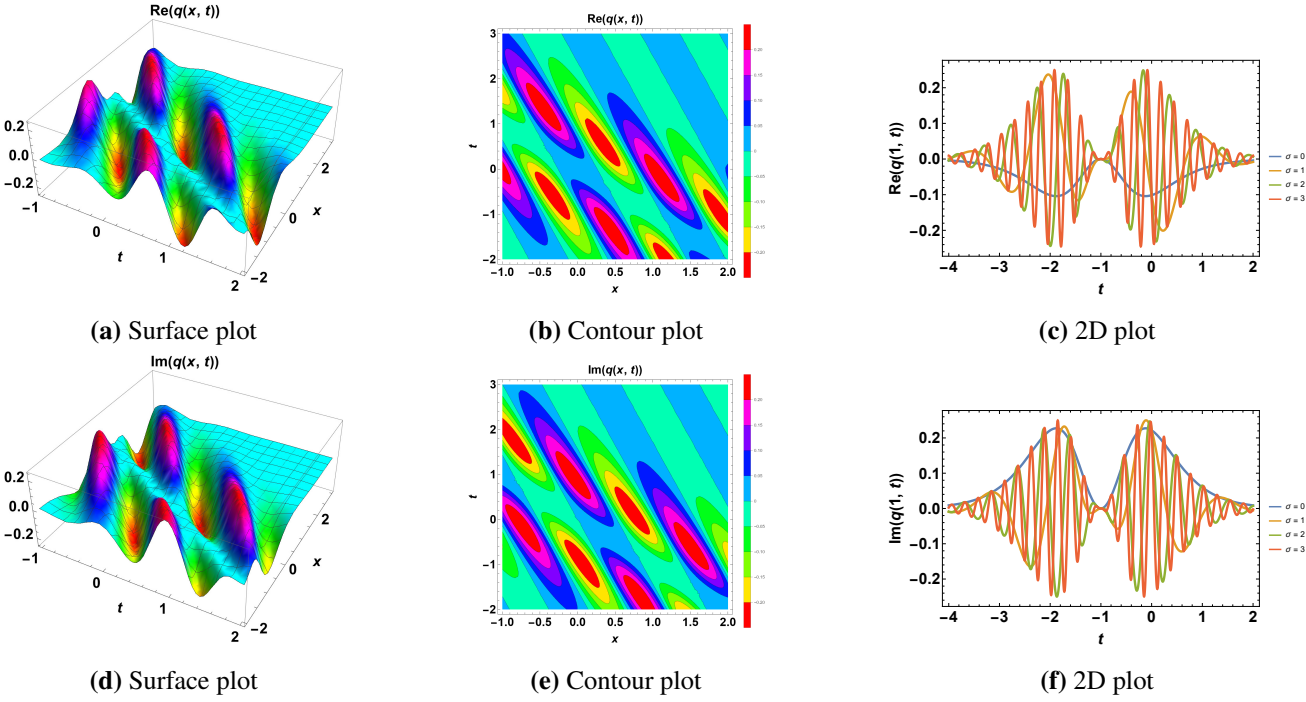
Figure 27. Profile of a bright-dark soliton given $\sigma = 3$.

(a) Surface plot

(b) Contour plot

(c) 2D plot

(d) Surface plot

(e) Contour plot

(f) 2D plot
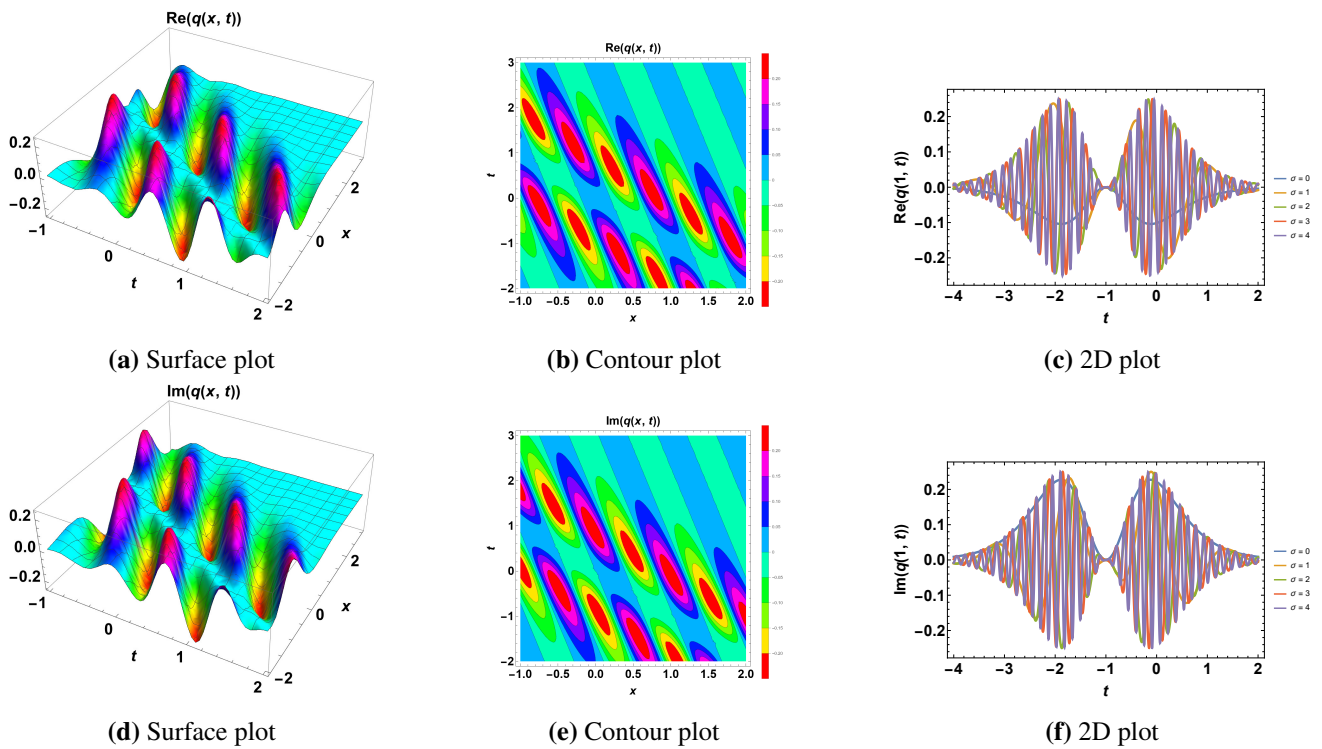
Figure 28. Profile of a bright-dark soliton given $\sigma = 4$.

(a) Surface plot

(b) Contour plot

(c) 2D plot

(d) Surface plot

(e) Contour plot

(f) 2D plot
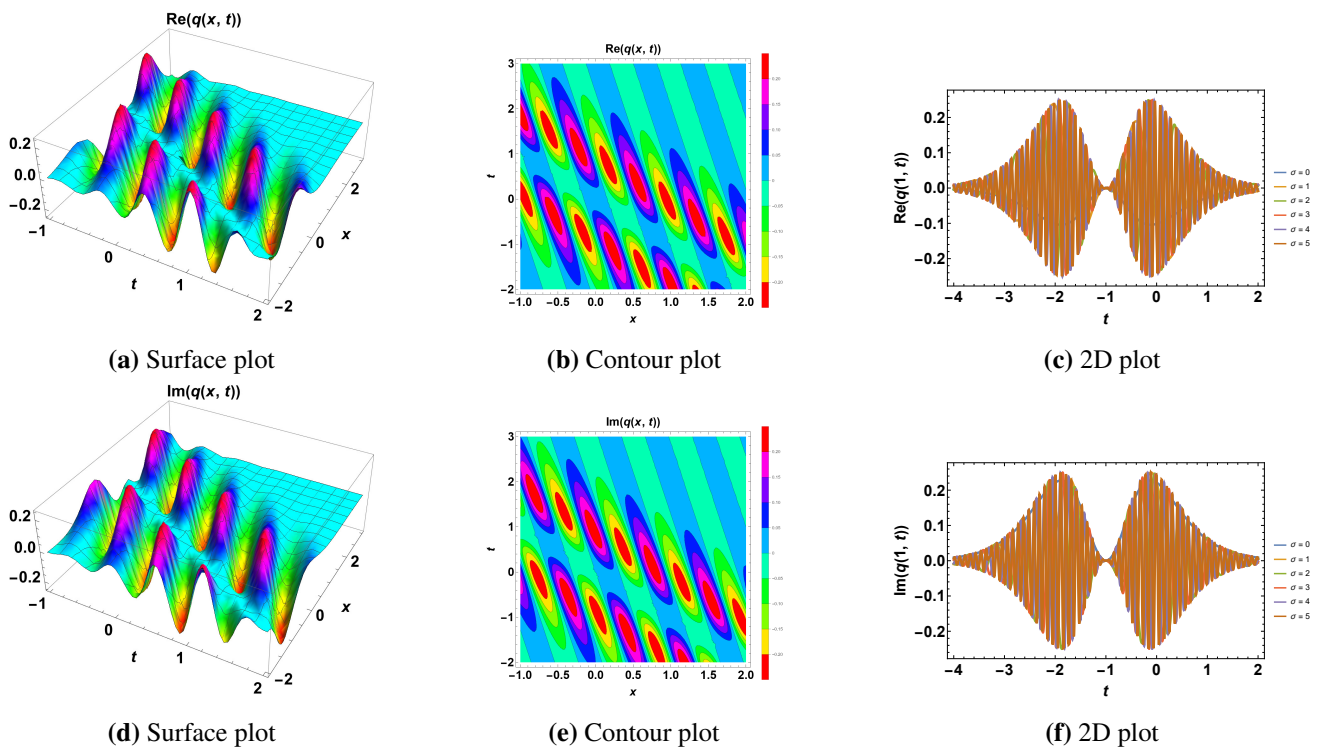
Figure 29. Profile of a bright-dark soliton given $\sigma = 5$.

(a) Surface plot

(b) Contour plot

(c) 2D plot

(d) Surface plot

(e) Contour plot

(f) 2D plot
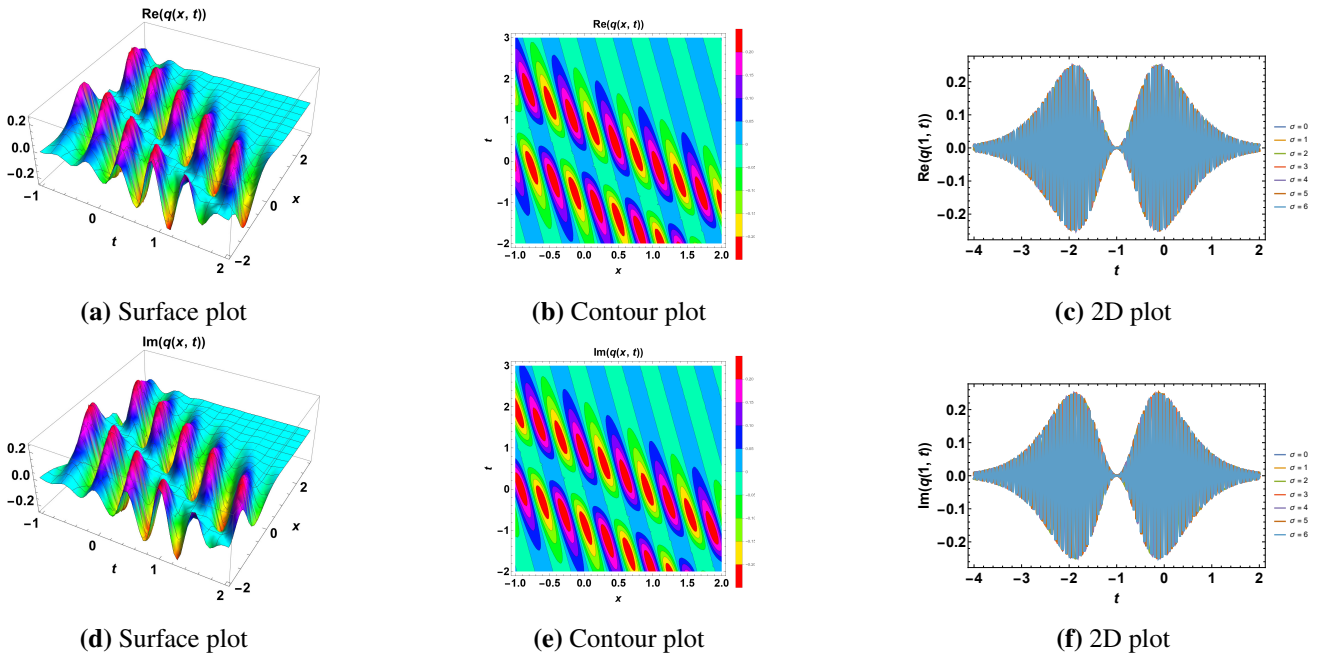
Figure 30. Profile of a bright-dark soliton given $\sigma = 6$.

(a) Surface plot

(b) Contour plot

(c) 2D plot

(d) Surface plot

(e) Contour plot

(f) 2D plot

(g) Surface plot

(h) Contour plot

(i) 2D plot
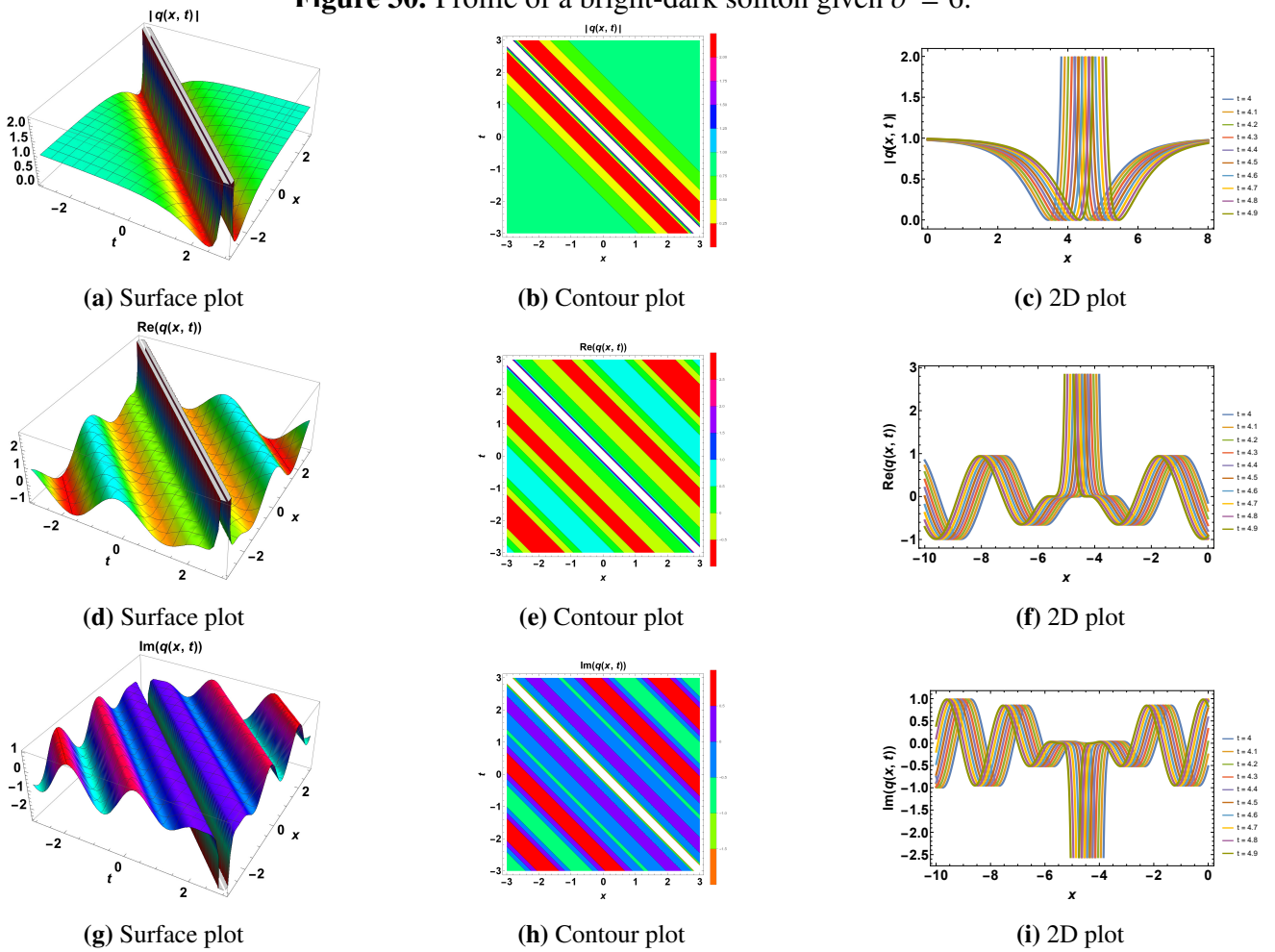
Figure 31. Profile of a singular-singular soliton given $\sigma = 0$.

(a) Surface plot   **(b)** Contour plot   **(c)** 2D plot

(d) Surface plot   **(e)** Contour plot   **(f)** 2D plot
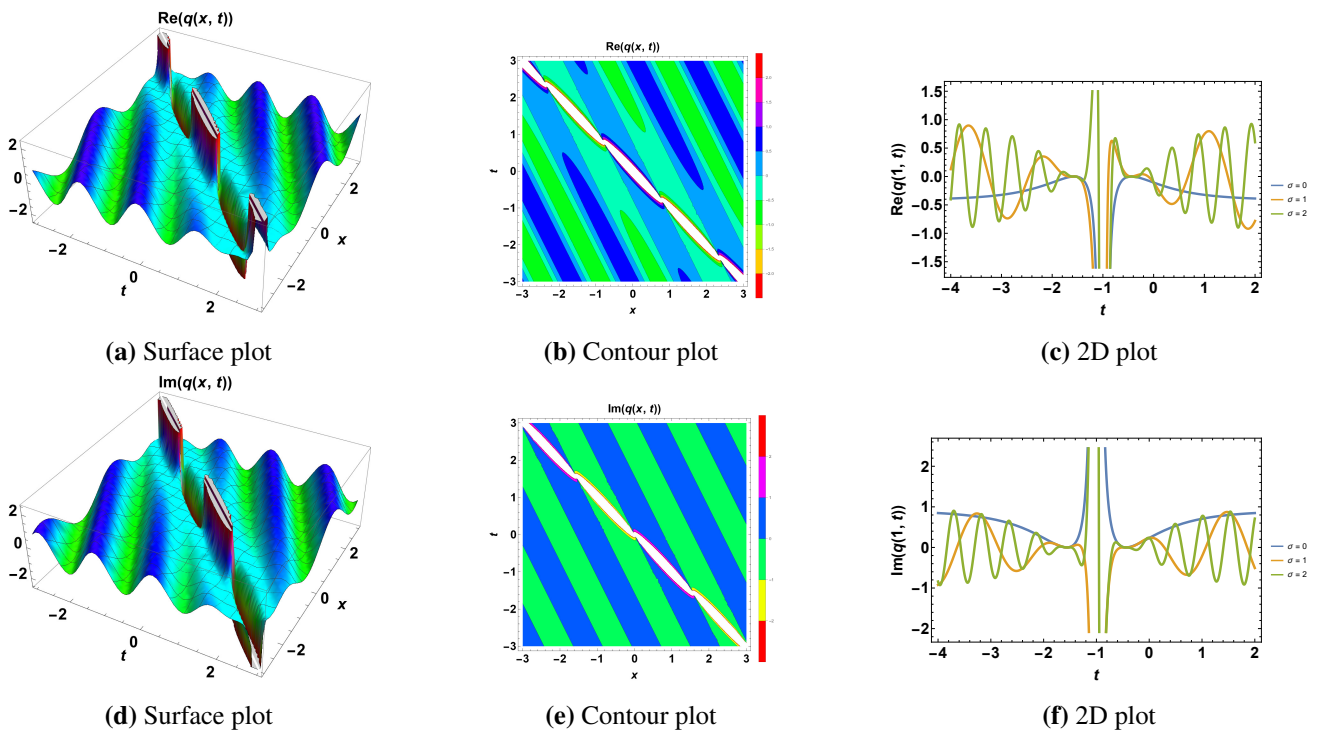
Figure 32. Profile of a singular-singular soliton given $\sigma = 2$.

(a) Surface plot   **(b)** Contour plot   **(c)** 2D plot

(d) Surface plot   **(e)** Contour plot   **(f)** 2D plot
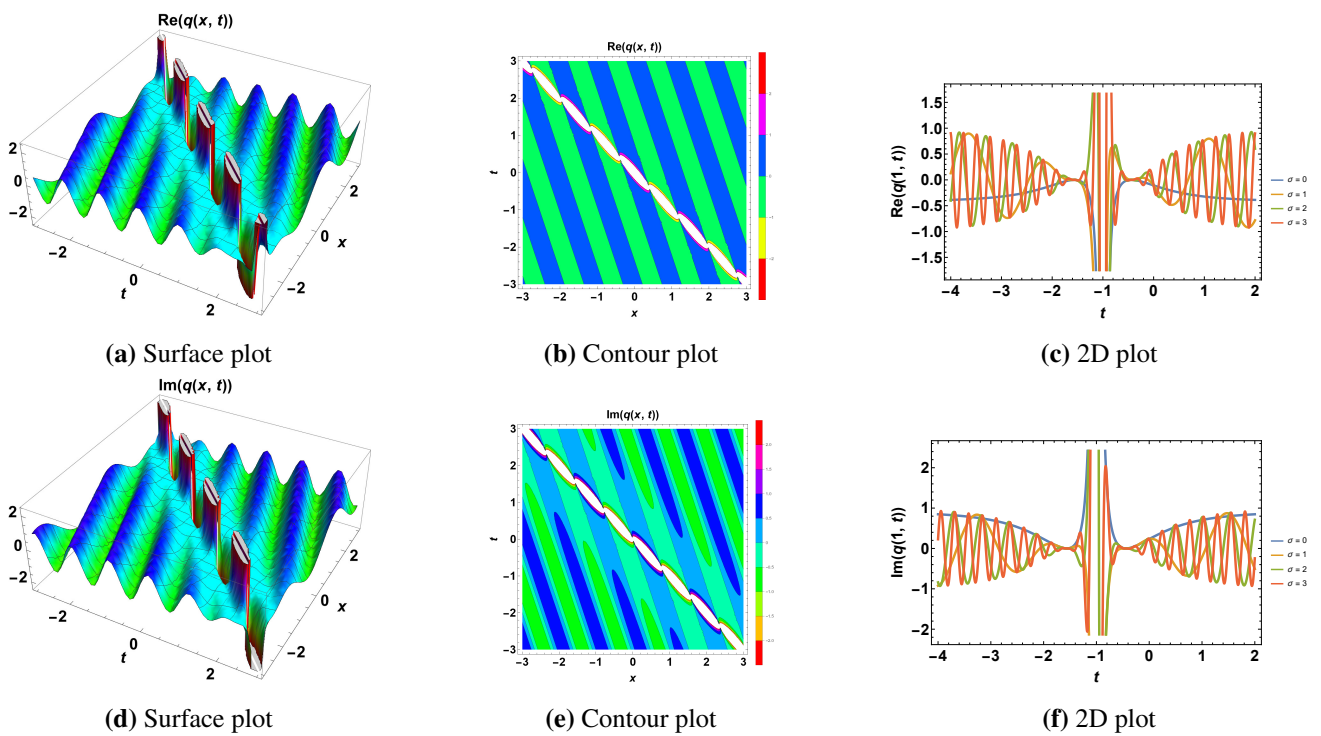
Figure 33. Profile of a singular-singular soliton given $\sigma = 3$.

(a) Surface plot

(b) Contour plot

(c) 2D plot

(d) Surface plot

(e) Contour plot

(f) 2D plot
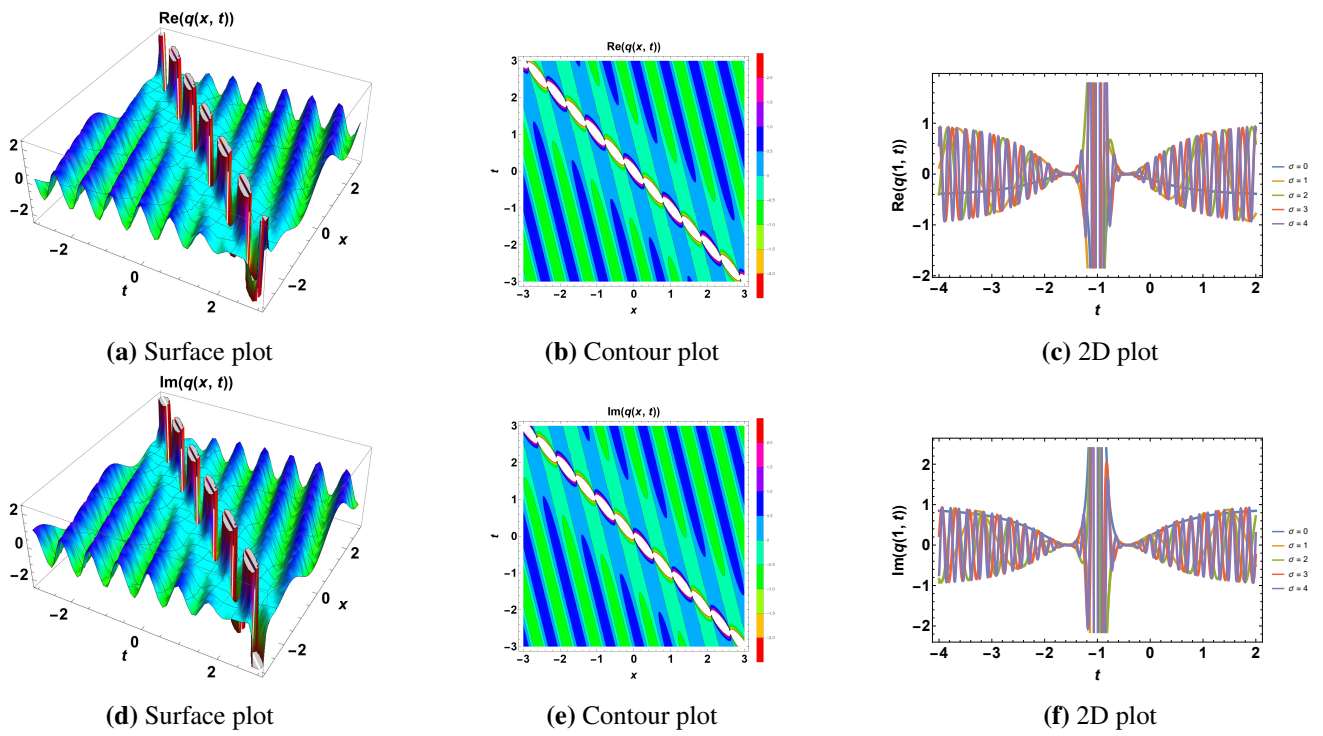
Figure 34. Profile of a singular-singular soliton given $\sigma = 4$.

(a) Surface plot

(b) Contour plot

(c) 2D plot

(d) Surface plot

(e) Contour plot

(f) 2D plot
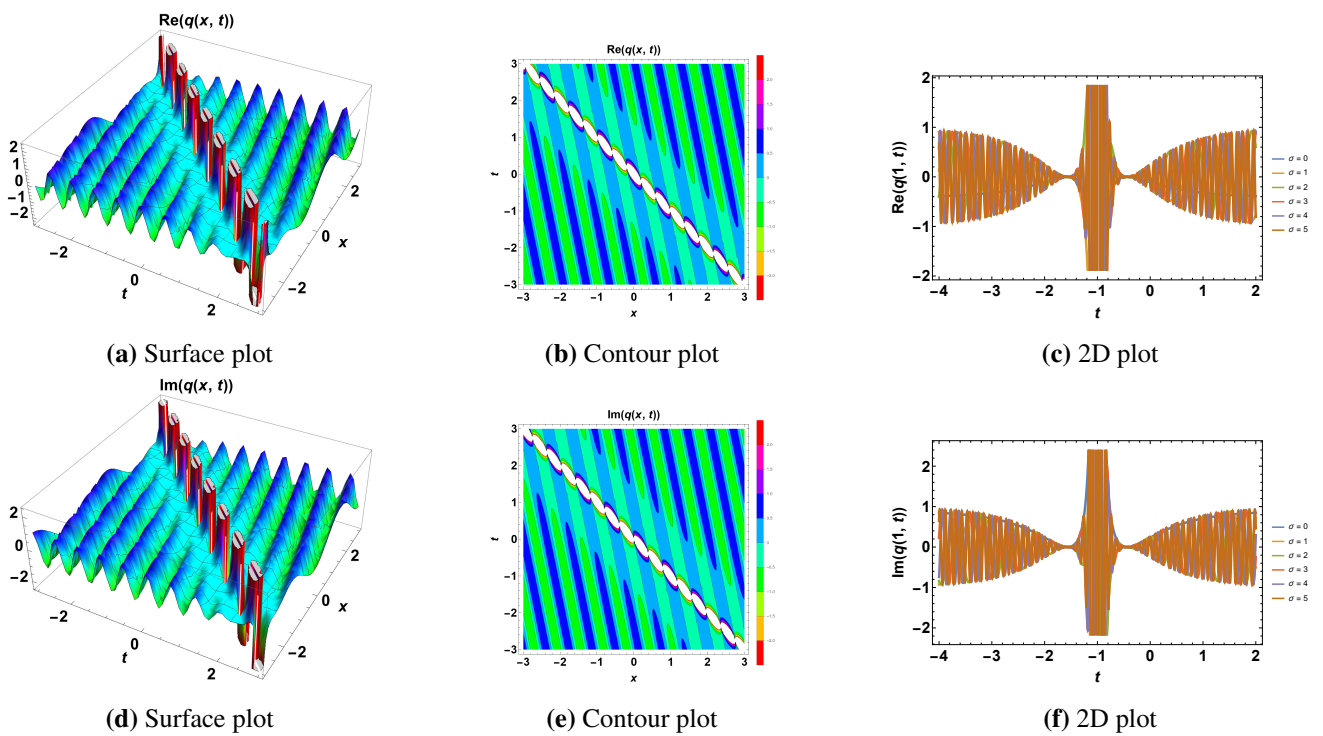
Figure 35. Profile of a singular-singular soliton given $\sigma = 5$.
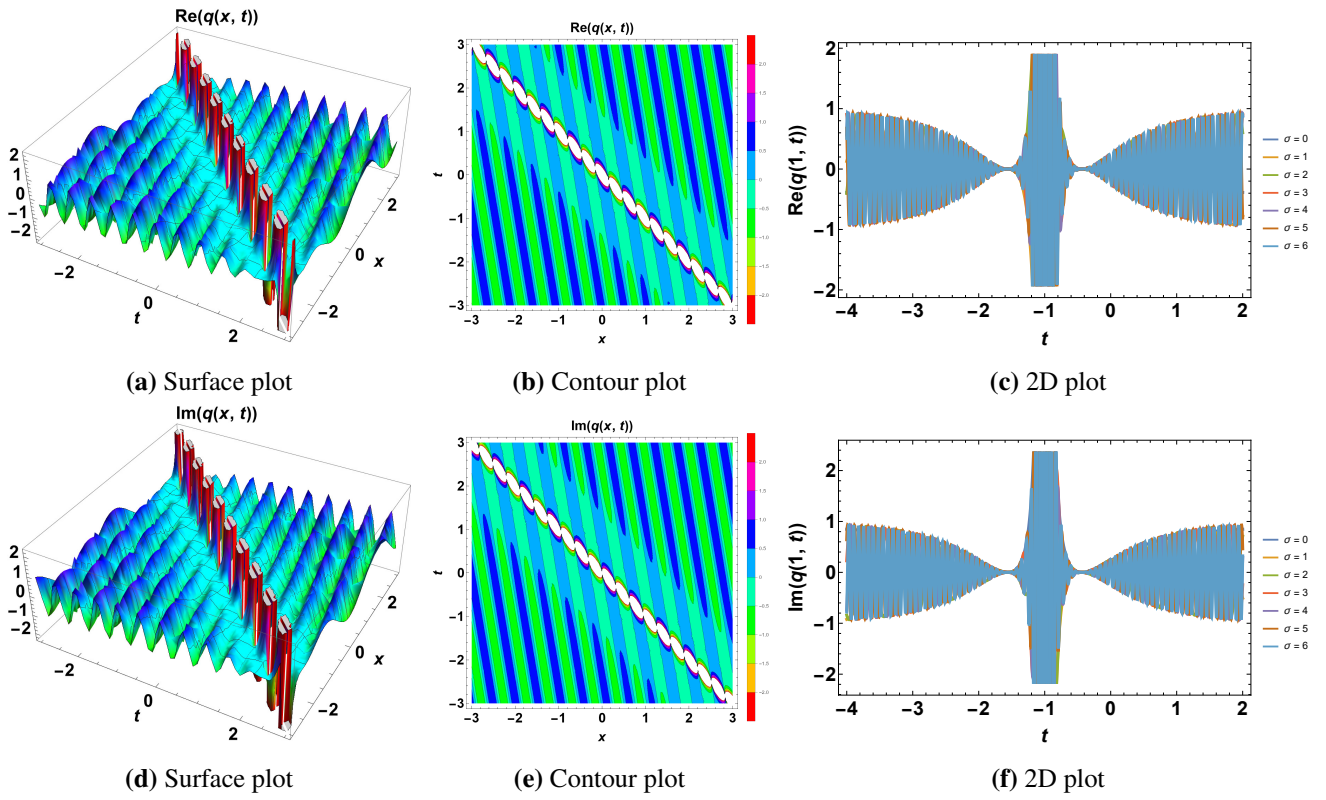
Figure 36. Profile of a singular-singular soliton given $\sigma = 6$.
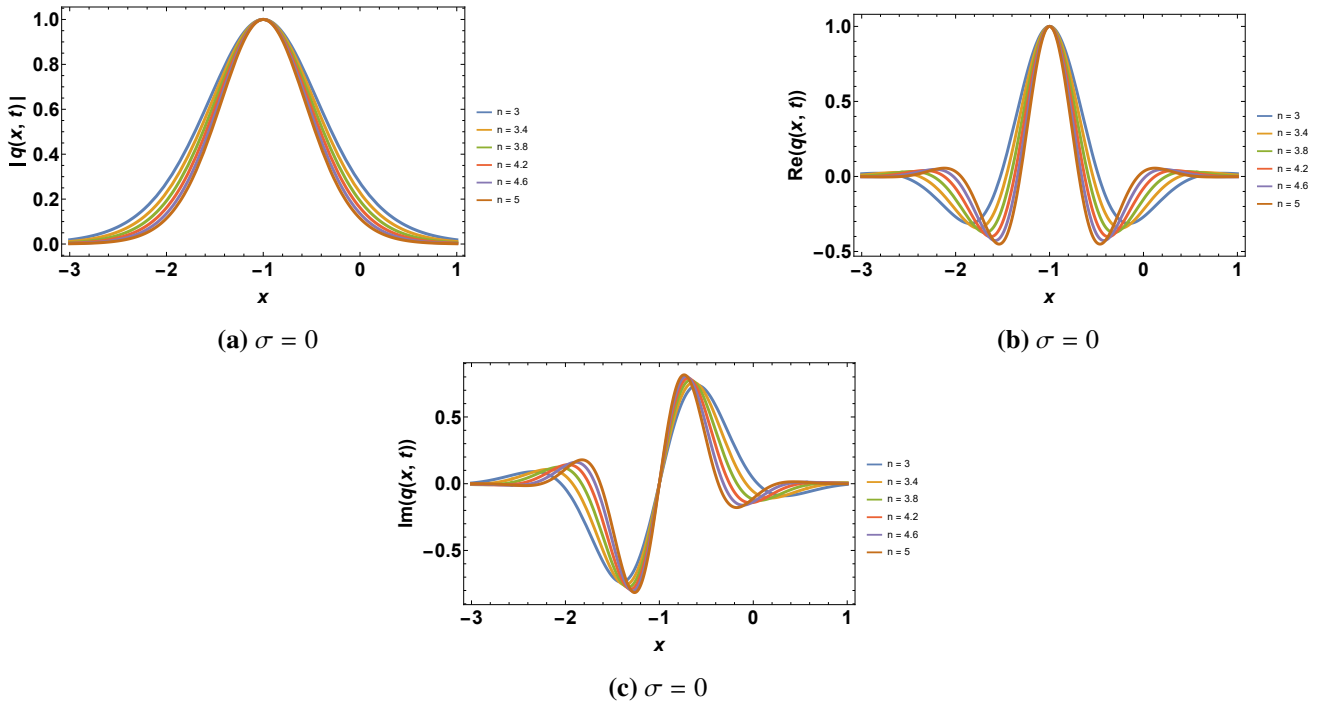
Figure 37. Profile of a bright soliton given $\sigma = 0$.
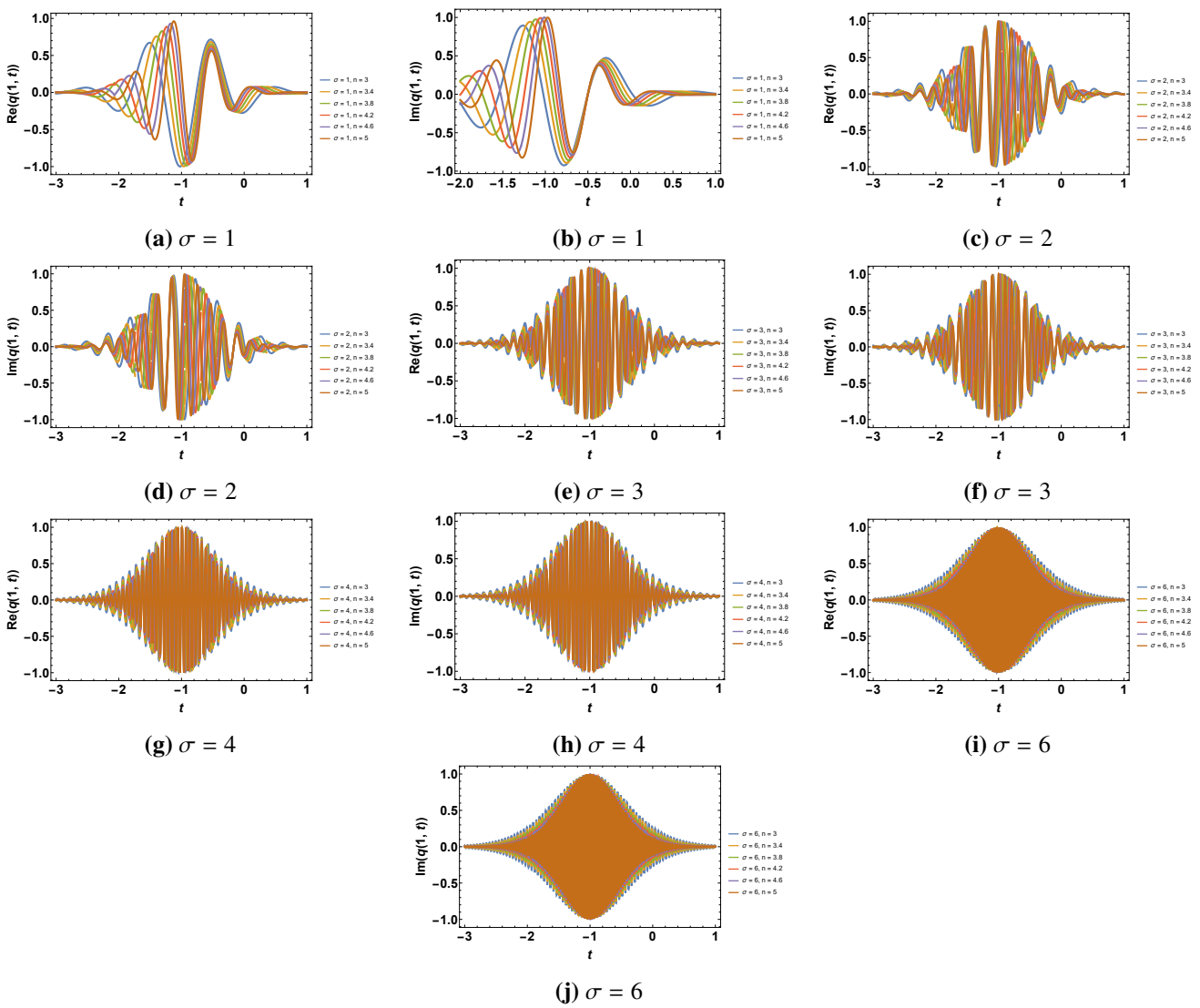
Figure 38. Profile of a bright soliton given $\sigma = 6$.
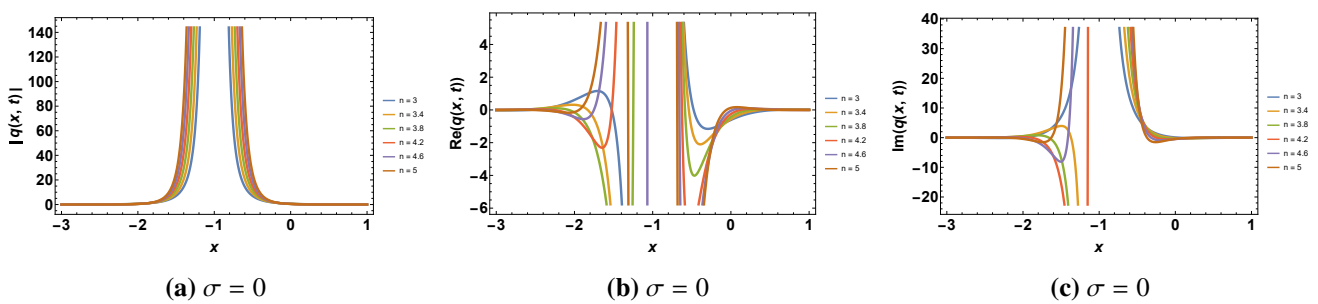
Figure 39. Profile of a singular soliton given $\sigma = 0$.
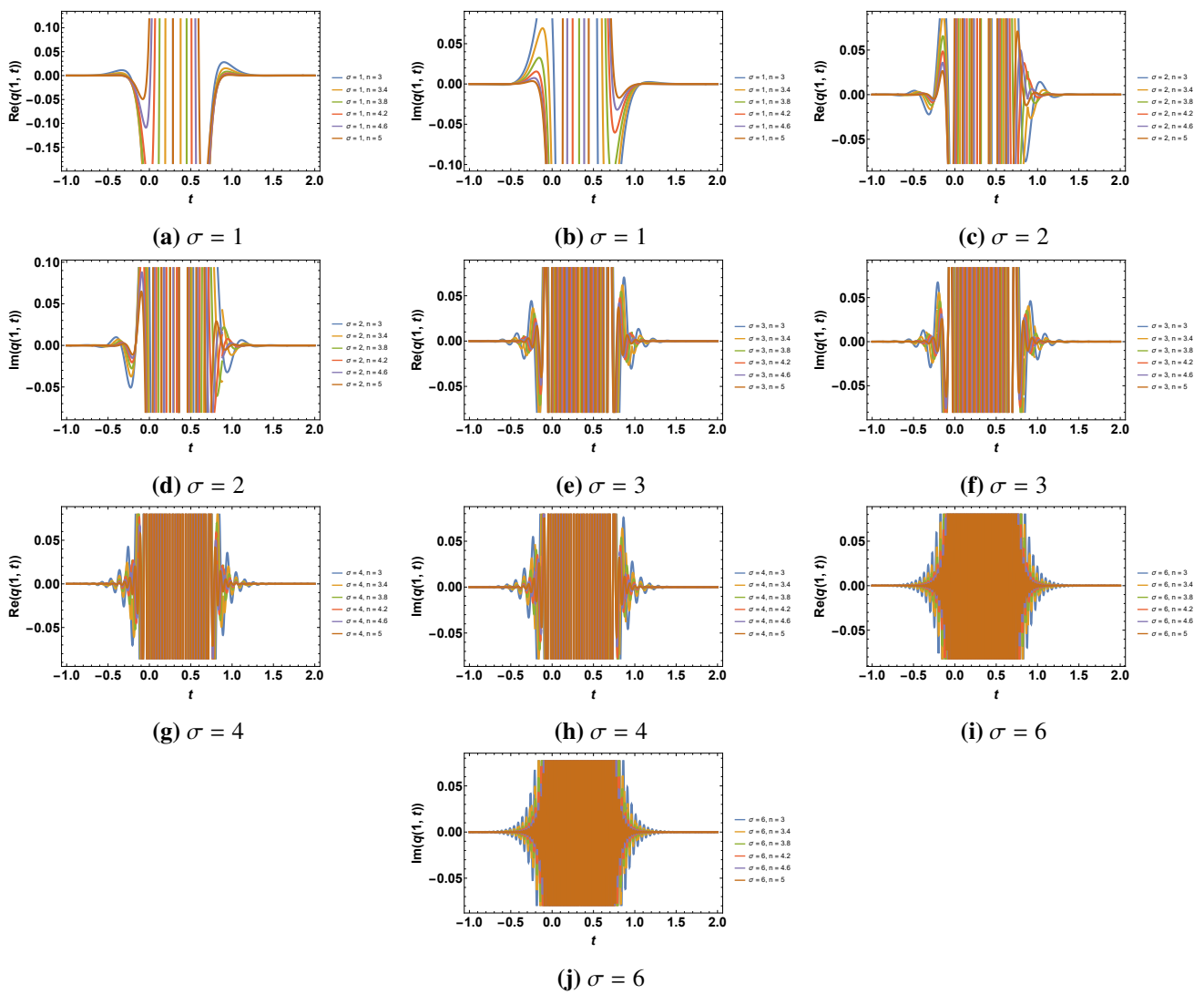
Figure 40. Profile of a singular soliton given $\sigma = 6$.